

# Loss and gain of *Drosophila* TDP-43 impair synaptic efficacy and motor control leading to age-related neurodegeneration by loss-of-function phenotypes

Danielle C. Diaper<sup>1,†</sup>, Yoshitsugu Adachi<sup>1,†</sup>, Ben Sutcliffe<sup>3</sup>, Dickon M. Humphrey<sup>1</sup>, Christopher J.H. Elliott<sup>4</sup>, Alan Stepto<sup>1</sup>, Zoe N. Ludlow<sup>1</sup>, Lies Vanden Broeck<sup>5</sup>, Patrick Callaerts<sup>5</sup>, Bart Dermaut<sup>5,6</sup>, Ammar Al-Chalabi<sup>2</sup>, Christopher E. Shaw<sup>2</sup>, Iain M. Robinson<sup>3</sup> and Frank Hirth<sup>1,\*</sup>

<sup>1</sup>Department of Neuroscience and <sup>2</sup>Department of Clinical Neuroscience, Institute of Psychiatry, MRC Centre for Neurodegeneration Research, King's College London, London SE5 8AF, UK, <sup>3</sup>Peninsula College of Medicine and Dentistry, Universities of Exeter and Plymouth, Plymouth PL6 8BU, UK, <sup>4</sup>Department of Biology, University of York, York YO10 5DD, UK, <sup>5</sup>Laboratory of Behavioural & Developmental Genetics, Centre for Human Genetics, University of Leuven & VIB Centre for the Biology of Disease, Leuven 3000, Belgium and <sup>6</sup>INSERM U744, Pasteur Institute of Lille, University of Lille North of France, Lille, France

Received January 2, 2013; Revised and Accepted January 3, 2013

**Cytoplasmic accumulation and nuclear clearance of TDP-43 characterize familial and sporadic forms of amyotrophic lateral sclerosis and frontotemporal lobar degeneration, suggesting that either loss or gain of TDP-43 function, or both, cause disease formation. Here we have systematically compared loss- and gain-of-function of *Drosophila* TDP-43, TAR DNA Binding Protein Homolog (TBPH), in synaptic function and morphology, motor control, and age-related neuronal survival. Both loss and gain of TBPH severely affect development and result in premature lethality. TBPH dysfunction caused impaired synaptic transmission at the larval neuromuscular junction (NMJ) and in the adult. Tissue-specific knockdown together with electrophysiological recordings at the larval NMJ also revealed that alterations of TBPH function predominantly affect pre-synaptic efficacy, suggesting that impaired pre-synaptic transmission is one of the earliest events in TDP-43-related pathogenesis. Prolonged loss and gain of TBPH in adults resulted in synaptic defects and age-related, progressive degeneration of neurons involved in motor control. Toxic gain of TBPH did not downregulate or mislocalize its own expression, indicating that a dominant-negative effect leads to progressive neurodegeneration also seen with mutational inactivation of TBPH. Together these data suggest that dysfunction of *Drosophila* TDP-43 triggers a cascade of events leading to loss-of-function phenotypes whereby impaired synaptic transmission results in defective motor behavior and progressive deconstruction of neuronal connections, ultimately causing age-related neurodegeneration.**

## INTRODUCTION

Tar DNA binding protein of 43 kDa (TDP-43) has been identified as the major disease protein present in cytoplasmic inclusions in amyotrophic lateral sclerosis (ALS) and frontotemporal lobar degeneration (FTLD). Full length TDP-43 protein as well as 25 kDa, C-terminal fragments were found

to be hyper-phosphorylated and ubiquitinated in aggregates present in affected brain and spinal cord of ALS and FTLD cases (1,2). TDP-43 inclusions are found as secondary histopathological feature in other neurodegenerative disorders including Alzheimer's, Parkinson's and Huntington's disease, thereby defining a novel proteinopathy (3,4). Dominant

\*To whom correspondence should be addressed at: Department of Neuroscience, Institute of Psychiatry, King's College London, PO Box 37, 16 De Crespigny Park, SE5 8AF London, UK. Tel: +44 2078480786; Fax: +44 2077080017; Email: frank.hirth@kcl.ac.uk

<sup>†</sup>The authors wish it to be known that, in their opinion, the first two authors should be regarded as joint First Authors.

missense mutations in the *TARDBP* gene have been identified in familial and sporadic cases of ALS and FTL (5–8), indicating that TDP-43 dysfunction may cause disease formation.

TDP-43 encodes an evolutionarily conserved protein comprising a bipartite nuclear localization signal, two RNA recognition motifs (RRMs), a nuclear export signal, a glycine and glycine/glutamine/asparagine-rich C-terminal region. The C-terminus resembles a prion-like domain (9,10) predominantly mutated in TDP-43-related ALS and FTL cases (11,12). *In vitro* studies showed that TDP-43 is involved in transcriptional regulation, RNA biogenesis and splicing (13). The C-terminal domain of TDP-43 regulates tissue-specific gene expression, transcriptional repression, and alternative splicing, and is essential for binding to heterogeneous nuclear ribonucleoproteins involved in microRNA and mRNA biogenesis, as well as RNA turnover (12,13).

The pathophysiological role of TDP-43 has been addressed in cell culture and animal models using mutation, alteration or expression of disease-specific variants of TDP-43 and its homologs in worms, flies, zebrafish, mice and rats (11,12,14). These studies revealed that post-translational modification (phosphorylation, ubiquitylation), truncation, mislocalization, nuclear clearance, cytoplasmic accumulation and defective autoregulation can all impact either directly or indirectly onto TDP-43 toxicity (12). The resulting phenotypes include lethality or reduced lifespan, defects in axogenesis and neurite branching, altered synaptic morphology, axon and neuron degeneration, astrogliosis, defective fat metabolism, impaired motor behavior and cognitive deficits (11,14). The available data suggest that TDP-43 toxicity is either directly or indirectly related to disease formation. So far, however, no consensus has emerged as to whether loss (i.e. nuclear clearance) or toxic gain (i.e. cytoplasmic accumulation) of TDP-43, or both, are causally related to disease onset and progression. Moreover, despite the fact that a large number of TDP-43 RNA targets have been identified (15–18), the initiating events and pathogenic pathways underlying TDP-43-mediated neurodegeneration remain to be identified.

Here we show that similar to its human homolog, *Drosophila* TDP-43, TAR DNA binding protein homolog (TBPH), is expressed in neurons, glia and muscle cells. Both loss of function and overexpression of TBPH result in decreased viability, impaired synaptic transmission, defective locomotion and age-related progressive neurodegeneration. Together these data suggest that both increased and decreased levels of TDP-43 initiate a loss-of-function phenotype, resulting in decreased neuronal viability and subsequent degenerative cell loss that characterize motor neuron diseases like ALS and FTL.

## RESULTS

### *Drosophila* TDP-43, TBPH, is expressed in neurons, glia and muscle cells

BLAST search of the annotated *Drosophila melanogaster* genome identified two genes with sequence similarities to TARDBP/TDP-43, namely *TBPH* (19) and *CG7804*. Genomic sequence analysis revealed that the predicted six isoforms of *TBPH* are encoded by 5–6 exons, whereas the coding region of *CG7804* is intronless with sequence similarity to

exon 1–4 of *TBPH*. The differences in exon–intron structure and coding sequence similarities between *CG7804* and *TBPH* suggest that *CG7804* is paralogous to *TBPH* and likely to be a newly evolved retrogene that derived from *TBPH* rather than *TARDBP* (20). Moreover, in contrast to *TBPH*, *CG7804* is not expressed in CNS and lacks a prion-like C-terminus that is predominantly mutated in ALS and FTL (Supplementary Material, Fig. S1). We therefore focused on *TBPH*.

We generated polyclonal antibodies against *TBPH*-specific peptide sequences. Western blot analysis of control tissue identified a 58 kDa protein encoded by *TBPH* which was absent in deletions uncovering the genomic locus (Supplementary Material, Fig. S2); we did not detect any cleavage products, *TBPH* fragments, dimers nor band that indicates post-translational modifications (Supplementary Material, Fig. S2). Whole-mount immunocytochemistry revealed that, similar to human TDP-43, *TBPH* is expressed throughout development and adulthood in the nucleus of neurons, glia and muscle cells (Fig. 1). Perinuclear, cytoplasmic *TBPH* expression was detectable in post-mitotic neurons (Fig. 1L–O), although immunoreactivity was less intense than nuclear anti-*TBPH* labeling. These data suggest that similar to TDP-43, and predicted by nuclear localization and export signals (21,22), *TBPH* is predominantly localized to the nucleus but also shuttles into the cytoplasm.

### Both loss and gain of *TBPH* affect survival and motor behavior

To study TDP-43 dysfunction in *Drosophila*, we generated specific loss- and gain-of-function alleles of *TBPH*. Imprecise P-element excision resulted in two independent deletions that removed the promoter region and start codon, or the promoter region, start codon, exons 1–3 and parts of exon 4 coding for the *TBPH* RRM (Fig. 2A). RT–PCR and western blot analyses determined the absence of *TBPH* RNA and protein (Fig. 2B and C). For tissue-specific *TBPH* LOF, we generated two independent hairpin-loop UAS-RNAi lines that target exon 5 of all predicted *TBPH* isoforms (Supplementary Material, Fig. S3). BLAST search confirmed that our chosen target sequences do not detect off-targets, in contrast to other available *TBPH* RNAi lines, and western blot analysis revealed that *Tub-Gal4* driven *UAS-TBPH-RNAi* is able to knock down endogenous *TBPH* protein expression below detection level (Supplementary Material, Fig. S3).

For gain of *TBPH* function (GOF), several independent UAS lines were generated with single inserts on different chromosomal locations. Expression efficacy was tested using eye-specific *GMR-Gal4* activation. Western blot analysis revealed that *GMR>TBPH* showed increased amounts of *TBPH* protein (Fig. 2D) comparable among different insertion lines (Fig. 2E). Targeted misexpression resulted in excessive accumulation of *TBPH* both in the nucleus and cytoplasm (Supplementary Material, Fig. S4).

Analysis of zygotic *TBPH* LOF (*TBPH*<sup>–/–</sup>) and Gal4-mediated GOF mutants revealed that both affect development and lifespan: only 10–20% of progeny eclosed as adult while the majority of mutant cases died during late larval/pupal stages (Fig. 3A). Adult *TBPH*<sup>–/–</sup> mutant and pan-neuronal Gal4-specific *ELAV>TBPH* GOF flies were characterized by

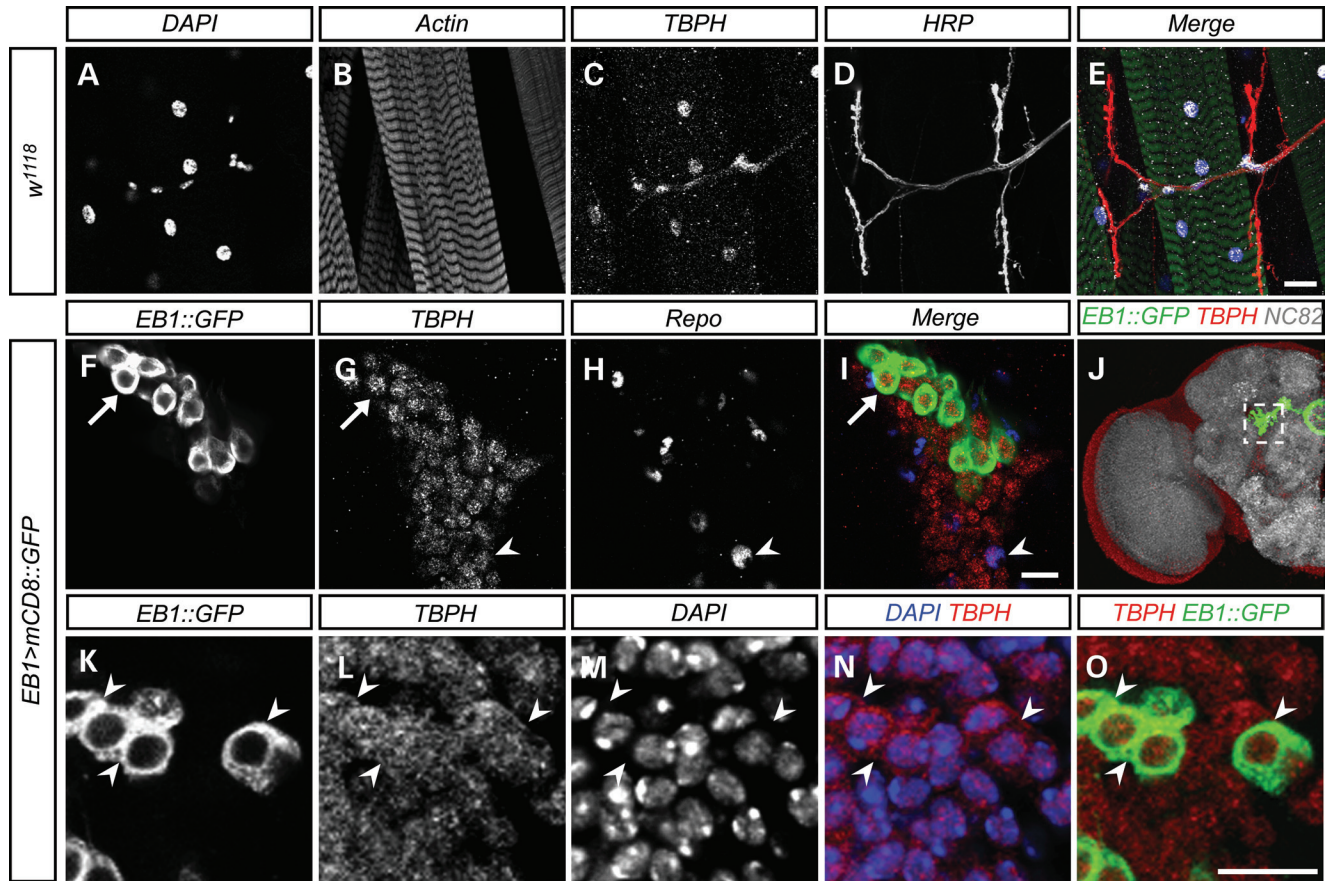


**Figure 1.** TBPH is expressed in neurons, glia and muscle cells. (A–E) Endogenous TBPH expression was examined at the neuromuscular junction of muscle group 6/7 of abdominal segment II in *w<sup>1118</sup>* wandering third instar larvae. TBPH is expressed in the nucleus of muscle cells (C–E). Images are z-projections of a 10 μm area scanned in 2 μm steps. (F–J) Endogenous TBPH expression was examined in the adult brain of flies expressing membrane-bound GFP in ellipsoid body neurons of the central brain that are considered to be upper motor neurons [*EB1>mCD8::GFP*; CNS hemisphere shown in (J), the dotted white box corresponds to (F–I)]. TBPH is expressed in neurons (F and G, arrow) and glia (H, arrowhead) throughout the adult brain, including ellipsoid body neurons. Images are single z-slices taken in 1 μm steps. (K–O) TBPH expression is also seen in perinuclear regions of ellipsoid body neurons as shown by its co-localization with membrane bound mCD8::GFP (white arrowheads). Images are single z-sections taken in 1.5 μm steps. Scale bars; 50 μm (A–E); 10 μm (F–I, K–O).

shortened lifespan, with *TBPH*<sup>-/-</sup> adults dying around day 7 and pan-neuronal Gal4-specific *ELAV>TBPH* flies dying around day 35, when compared with wild-type controls with an average lifespan of 80 days (23,24) (data not shown). Affected larvae exhibited impaired peristalsis and defective locomotion, which was more severe in *TBPH*<sup>-/-</sup> LOF mutants compared with pan-neuronal Gal4-specific *ELAV>TBPH* GOF (Fig. 3B). Adult *TBPH*<sup>-/-</sup> LOF mutant escapers and pan-neuronal Gal4-specific *ELAV>TBPH* GOF flies were characterized by inexistent or severely impaired innate escape and climbing behaviors (Fig. 3C).

To further investigate motor behavior, we used an open-field paradigm together with video-assisted motion tracking (23,24) (Fig. 3D) and compared adult *TBPH*<sup>-/-</sup> mutant LOF escapers with *EB1-Gal4*-mediated *UAS-TBPH* GOF flies targeting TBPH to ellipsoid body neurons of the central complex that are upper motor neurons due to their prominent role in the higher control of locomotion (25). Analysis of adult *TBPH*<sup>-/-</sup> mutant LOF escapers and *EB1>TBPH* GOF flies revealed severely reduced walking activity and distance traveled; motor activity remained low over time with only *TBPH*<sup>-/-</sup> flies walking slower (Fig. 3D–H). In addition,

both LOF and GOF flies were characterized by severe gait abnormalities (Fig. 3I). These data suggest that TBPH dysfunction affects lifespan and motor behavior.

To confirm that the phenotypes observed in homozygous *TBPH*<sup>-/-</sup> LOF flies were indeed due to the absence of TBPH, we carried out a complementation test using a deficiency line uncovering the genomic region of chromosome 2R (*Df(2R)106*) including the TBPH locus, which revealed early larval lethality suggesting non-complementation. In addition and to rule out hidden second-site mutations, we first analyzed heteroallelic combinations using our *TBPH<sup>DD96</sup>* and *TBPH<sup>DD100</sup>* alleles together with a recently reported deletion (26), which also revealed non-complementation. Secondly, we generated a genomic TBPH construct covering the entire coding region of TBPH as well as 3'- and 5'- regions upstream of the TBPH locus (Supplementary Material, Fig. S5). To analyze its rescue potential, we integrated *TBPH<sup>genomic</sup>* on 3R using the attP86Fb landing site and crossed it into the *TBPH<sup>DD96</sup>* mutant background. Analysis of homozygous *TBPH<sup>DD96</sup>*<sup>-/-</sup> flies carrying one or two copies of *TBPH<sup>genomic</sup>* revealed full rescue. Thus, development, larval locomotion, eclosion, adult climbing, walking and tripod gait phenotypes



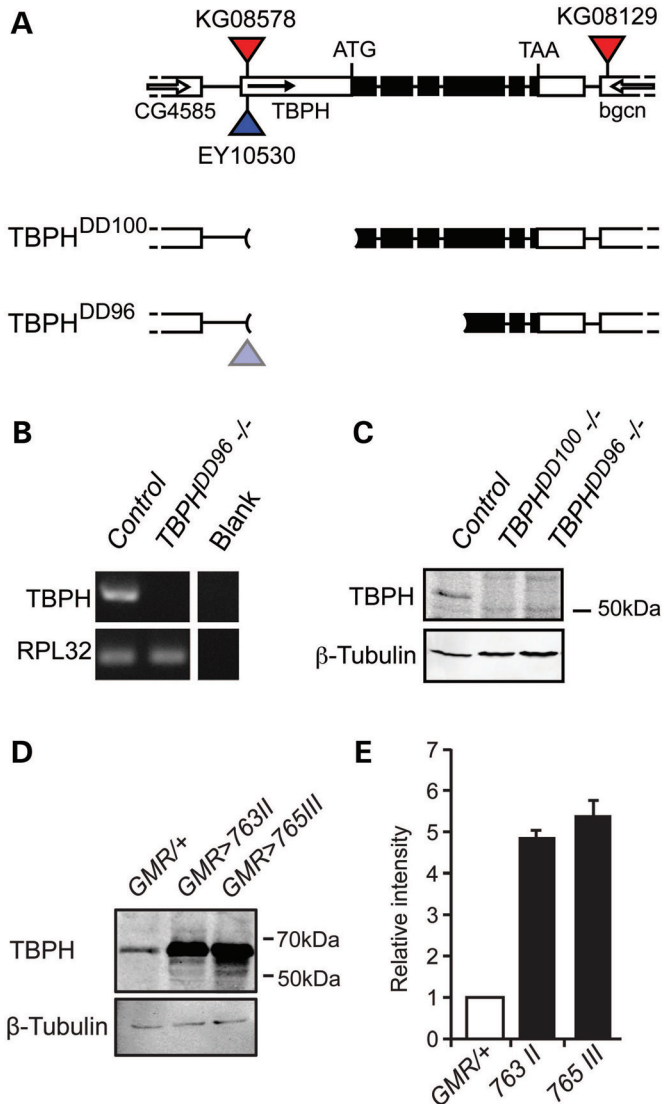


**Figure 2.** Loss- and gain-of-function alleles of the *Drosophila* TDP-43 homolog TBPH. (A–C) TBPH null mutant alleles and (D, E) UAS-TBPH overexpression alleles. (A) TBPH null mutant alleles ( $TBPH^{DD100}$  and  $TBPH^{DD96}$ ) were generated by imprecise P-element excision. Two types of deletion mutant were generated lacking distinct sections of the TBPH genomic region. The  $TBPH^{DD100}$  allele is lacking the promoter region of TBPH, including the start codon. The  $TBPH^{DD96}$  allele is lacking a larger amount of gDNA including the promoter region, the start codon and bases encoding the RNA recognition motifs (RRMs). (B) RT-PCR revealed lack of TBPH mRNA in homozygous TBPH mutants. Ribosomal protein L32 (RPL32) was used as loading control. Control genotype:  $w^{1118}$ . (C)  $TBPH^{DD100}$  and  $TBPH^{DD96}$  mutant alleles are protein null, as revealed by the absence of the TBPH-specific 58 kDa protein band present in  $w^{1118}$  flies (control); shown is a western blot using protein extracts from six fly heads blotted with anti-TBPH antibody. (D) Western blot analysis of GMR-Gal4 driven UAS-TBPH shows excess TBPH protein expression in adult heads. Two different UAS-TBPH lines with insertion on different chromosomes (#763 on II, #765 on III) show comparable expression levels. (E) Quantification of  $GMR>TBPH$  shows a dramatic increase in TBPH protein levels. Western blot TBPH signal intensities were normalized against  $\beta$ -Tubulin. Mean and SEM are shown.

of homozygous  $TBPH^{DD96}$  mutants were all restored in  $TBPH^{DD96-/-}; TBPH^{genomic}$  flies (Supplementary Material, Fig. S6). Together, these data suggest that the observed

loss-of-function phenotypes are indeed due to the loss of TBPH, and hence our  $TBPH^{-/-}$  mutants represent bona fide TBPH null alleles.

### TBPH dysfunction does not affect synapse morphology but function

To determine the cause of TBPH-mediated behavioral phenotypes, we analyzed whether TBPH dysfunction results in muscle defects. Phalloidin staining of either larval L3 or adult day 2  $TBPH^{-/-}$  muscle preparations revealed a muscle pattern indistinguishable of wild-type or heterozygous  $TBPH^{+/-}$  controls (data not shown). Next we investigated whether TBPH dysfunction may cause alterations of NMJ synapse structure and morphology, as previously suggested (27–30). We used a collection of synaptic markers (31) including *Fasciclin II* (*FasII*), involved in synapse development and plasticity; *Bruchpilot* (*NC82*), a component of the synaptic active zone of neurotransmitter release; *synaptotagmin* (*Syt*) involved in membrane traffic and calcium-dependent neurotransmitter release; *Futsch*, a pre-synaptic cytoskeletal protein that binds microtubules and regulates synaptic growth and dendritic morphology; and *Neuroglian* (*Nrg*), a cell surface, transmembrane adhesion molecule involved in motor neuron pathfinding. Larval NMJ preparations were double-labeled for synaptic proteins and horse radish peroxidase (HRP) that visualizes axons, dendrites and synaptic boutons in *Drosophila*. However, for all of the synaptic proteins examined, none were found to be mislocalized or absent in  $TBPH^{-/-}$  LOF larvae compared with age-matched  $w^{1118}$  controls (Supplementary Material, Fig. S7). A quantitative analysis of HRP-labeled synaptic boutons and active zone puncta immunolabeled by anti-Bruchpilot, did not reveal any indication for alterations in the number of synaptic boutons or anti-Bruchpilot positive active zones in homozygous  $TBPH^{DD96-/-}$  LOF larvae compared with age-matched  $w^{1118}$  controls (Supplementary Material, Fig. S8). These data suggest that the observed TBPH-related larval motor phenotypes are not caused by morphological defects, mislocalization or loss of selected proteins involved in synapse formation and maintenance.

We then carried out electrophysiological recordings of cases and controls to address whether TBPH-mediated behavioral phenotypes might be caused by defects in synaptic efficacy and function. Electrophysiological recordings made at the NMJ of homozygous  $TBPH^{DD96-/-}$  LOF and pan-neuronal Gal4-mediated  $ELAV>TBPH$  GOF L3 larvae revealed a decrease in both the amplitude and frequency of miniature excitatory junction potentials (mEJPs) in the homozygous loss-of-function background. Low-frequency (0.2 Hz) stimulation of the NMJ showed no difference in evoked excitatory junction potential (EJP) amplitudes. As a consequence of the changed mini amplitude but unaltered EJP amplitude there was an increase in the quantal content in TBPH LOF but not in  $ELAV>TBPH$  GOF (Fig. 4A and B). No differences were seen during high-frequency stimulation between cases and controls (data not shown).

We also recorded electroretinograms (ERGs) from adult TBPH LOF and GOF cases compared with appropriate controls. Both white-eyed  $TBPH^{-/-}$  LOF and  $w^{1118}$  control



revealed similar responses to blue light pulses with no differences in peak–peak amplitude of the ERG. Moreover, the ERG amplitude of red-eyed *GMR>TBPH-RNAi* and OregonR were indistinguishable, also when compared between 1- and 5-day-old flies (Fig. 4C and D). We then examined the off-transient and plotted their size as a function of the maintained photoreceptor response. On average, data points from both TBPH LOF strains, *TBPH-/-* and *GMR>TBPH-RNAi* flies, were above those from controls (Fig. 4E). We tested the null hypothesis that data points were distributed evenly above and below the control regression line between maintained ERG potential and off-transient, which revealed significant deviation for both *TBPH-/-* and *GMR>TBPH-RNAi*. Moreover, we compared the size of the off-transient recorded in both TBPH LOF lines with that estimated from the control regression line which revealed 15 and 25% reduction in the off-transient in *TBPH-/-* and *GMR>TBPH-RNAi*, respectively. As positive control, we blocked synaptic transmission in the retina using *GMR>Shibire-RNAi*, the *Drosophila* homolog of Dynamin involved in synaptic transmission (32), which resulted in completely abolished off-transient (Fig. 4C) with data points significantly above the wild-type regression line (Fig. 4E).

We also recorded ERGs from TBPH GOF flies where *Drosophila* TDP-43 was over-expressed in the eye. *TBPH/w-* controls showed an ERG in response to blue light pulses like wild-type, whereas *GMR/w-* flies showed a smaller response. In contrast, *GMR>TBPH* GOF flies showed a very small response, with no off/on transients visible (Fig. 4F and G), suggesting reduced synaptic signaling. Taken together these data suggest that both TBPH LOF and GOF affect synaptic efficacy and function, which is also supported by an impaired innate escape response (Fig. 3C and Supplementary Material, Fig. S9). The observed differential effects on synaptic efficacy and function in TBPH LOF and GOF suggest that *Drosophila* TDP-43 dysfunction either impairs post-synaptic efficacy or alters the size or loading of synaptic vesicles, which is consistent with the observed behavioral phenotypes of TBPH LOF and GOF (Fig. 3).

### Pre-synaptic deficits are early phenotypes of dysfunctional TBPH

To gain further insights into TBPH-related synaptic transmission defects, we wondered whether TBPH dysfunction at the larval NMJ affects pre- or post-synaptic efficiency, or both. To address this question, we manipulated TBPH levels in a tissue-specific manner and focused on Gal4-mediated TBPH knockdown by using UAS-TBPH-RNAi in combination with *UAS-Dicer-2* expression, which enhances knockdown efficiency (33). For pre-synapse-specific knockdown at the larval NMJ, we carried out pan-neuronal Gal4-mediated *ELAV>Dcr2*, *TBPH-IR* knockdown, and for post-synaptic TBPH knockdown, we used muscle-specific, Gal4-mediated *BG57>Dcr2*, *TBPH-IR* knockdown, in both cases utilizing reportedly strong and specific Gal4 drivers (34,35). Effects of pre- or post-synaptic TBPH-RNAi were analyzed using electrophysiological recordings at the L3 larval NMJ (Supplementary Material, Fig. S10).

Recordings at the NMJ of pan-neuronal Gal4-mediated *ELAV>Dcr2*, *TBPH-IR* knockdown larvae revealed a decrease in both the amplitude and frequency of mEJPs. Low frequency (0.2 Hz) stimulation of the NMJ showed no difference in evoked EJP amplitudes. As a consequence of the changed mini amplitude but unaltered EJP amplitude, we observed an increase in the quantal content in *ELAV>Dcr2*, *TBPH-IR* larvae (Supplementary Material, Fig. S10A and B). These data suggest that, similar to recordings at the NMJ of homozygous *TBPH<sup>DD96</sup>-/-* L3 loss-of-function larvae, pan-neuronal Gal4-mediated *ELAV>Dcr2*, *TBPH-IR* knockdown leads to impaired synaptic transmission (compare Supplementary Material, Fig. S10A and B with Fig. 4A, B).

In contrast to pre-synaptic knockdown of TBPH, recordings at the NMJ of muscle-specific Gal4-mediated *BG57>Dcr2*, *TBPH-IR* L3 knockdown larvae did not reveal any significant alterations in either amplitude or frequency of mEJPs, when compared with controls (Supplementary Material, Fig. S10C and D). Low frequency (0.2 Hz) stimulation of the NMJ revealed a small but significant difference in evoked EJP amplitudes. However, we did not detect any significant differences in quantal content in *BG57>Dcr2*, *TBPH-IR* L3 knockdown larvae (Supplementary Material, Fig. S10C and D). Together, these data demonstrate that altered TBPH function causes defective pre-synaptic transmission at the larval NMJ, suggesting that impaired pre-synaptic efficacy is one of the earliest events in the etiology of *Drosophila* TDP-43-related pathogenesis.

### TBPH is essential for neuronal activity underlying motor behavior

To further dissect TBPH dysfunction, we focused on cell-type-specific LOF and GOF and carried out TBPH-RNAi together with *Dcr2* targeted by *Tubulin-Gal4*, which is ubiquitously and constitutively active during development, adulthood and aging (24), as well as pan-neuronal *Elav-Gal4* and *E1-Gal4* specific to upper motor neurons. *Tub>Dcr2*, *TBPH-IR* mimicked *TBPH* mutations, causing larval/pupal lethality with few adult escapers (data not shown) and a disturbed tripod gait (Fig. 3I). To rule out that *UAS-Dcr2* itself does cause a walking phenotype, we analyzed *Tub>Dcr2* flies which revealed no differences in walking activity, distance or activity over time when compared with controls (Supplementary Material, Fig. S11). Adult *Tub>Dcr2*, *TBPH-IR* flies displayed impaired motor behavior comparable to *TBPH<sup>DD96</sup>-/-* null mutants with severely reduced walking activity and distance traveled; their motor behavior remained limited over time with significantly reduced walking speed (Fig. 5), and walking was characterized by severe gait abnormalities (Fig. 3I). We observed similar motor phenotypes with Gal4-mediated UAS-TBPH-RNAi LOF targeted either to post-mitotic neurons (*Elav>Dcr2*, *TBPH-IR*) or to upper motor neurons (*E1>Dcr2*, *TBPH-IR*) (Fig. 5). Moreover, analysis of open-field locomotion revealed that upper motor neuron-specific TBPH GOF (*E1>TBPH*) and upper motor neuron-specific TBPH-RNAi knockdown (*E1>Dcr2*, *TBPH-IR*), resulted in similar phenotypes characterized by severely impaired motor behavior (Figs 3E–H and 5). These data suggest that both tissue-specific loss and gain of *Drosophila* TDP-43 function impair neuronal activity underlying essential motor behavior.

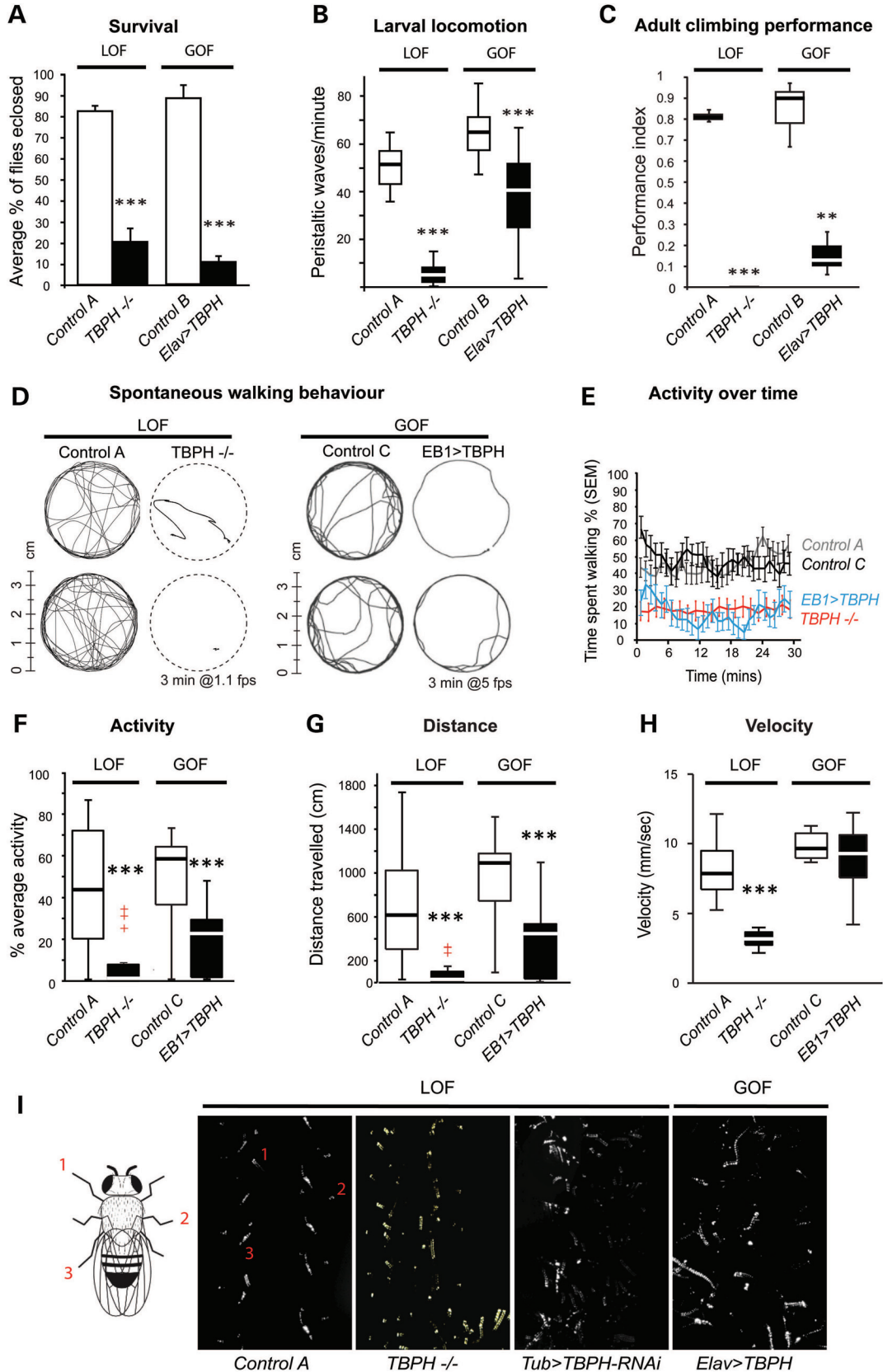


**Figure 3.** Both loss and gain of TBPH affect survival and motor behavior. (A) Survival analysis quantified the number of larvae that survived to adulthood. The number of fully eclosed adults was significantly reduced in loss-of-function (LOF) TBPH null mutants and gain-of-function (GOF) *ELAV>TBPH* flies, compared with respective control (*w<sup>1118</sup>/+*, control A; *Elav*+, control B). (B) Both TBPH LOF and GOF show impaired larval locomotion with a reduction in the

### TBPH dysfunction differentially affects synaptic integrity in an age-related manner

Next we investigated whether impaired synaptic activity caused by TBPH dysfunction may lead to synaptic alterations in aging flies. We therefore analyzed brains of aged flies with or without either *UAS-TBPH-IR* LOF or *UAS-TBPH* GOF targeted to *EB1-Gal4*-specific upper motor neurons. The *EB1-Gal4* driver becomes active during late pupal stages and remains active during adulthood and aging in a population of roughly 80 upper motor neurons (ellipsoid body ring neurons). In contrast to severe motor phenotypes (see Figs 3E–H and 5G–J), dysfunction or loss of this small population of upper motor neurons does not significantly alter the lifespan of flies and hence is an ideal assay system to study *Drosophila* TDP-43 dysfunction at the cellular and synaptic level (see Figs 6 and 7). We used *EB1-Gal4* driven *UAS-TBPH-IR* LOF or *UAS-TBPH* GOF and co-expressed a membrane-bound form of GFP (*UAS-mCD8::GFP*) that also visualizes axons and synaptic terminals, and co-labeled whole mount brains with anti-Fasciclin 2 (Fas2) that is also expressed at pre- and post-synaptic sites of the ellipsoid body ring neuropil (Supplementary Material, Fig. S12).

Analysis of brains of *Gal4*-mediated upper motor neuron-specific *EB1>Dcr2*, *TBPH-IR* at day 5, 20 and 40 did not reveal any significant differences at synaptic termini of the EB ring neuropil based on distribution, intensity, and shape of *mCD8::GFP* or Fas2 expression (Supplementary Material, Fig. S12A–J); however, by day 40, but not at day 5 or day 20, we consistently observed misshapen, fragmented and scattered cell bodies of EB ring neurons, together with a severe reduction in the number and fasciculation of axonal projections, when compared with age-matched controls (Supplementary Material, Fig. S12E–H, compare with Supplementary Material, Fig. S12A–D). In contrast, we observed strong reduction already by day 5 of *mCD8::GFP* labeling in cell body membranes, axons and synaptic termini of TBPH GOF brains (*EB1>mCD8::GFP*, *TBPH*), which was more pronounced by day 40; Fas2 immunoreactivity, however, appeared unaffected (Supplementary Material, Fig. S12K–T).

To determine in more detail whether the age-related synaptic alterations were either pre- or post-synaptic, we made use of the pre-synaptic marker *synaptotagmin* fused to GFP (*UAS-Syt::GFP*) in combination with the post-synaptic marker *DenMark*, a fusion protein of *telencephalin* and *mCherry*, which labels the somatodendritic compartment in *Drosophila* (36) (Fig. 6). Analysis of day 5, day 40 and day 50 adult *EB1>Syt::GFP*, *DenMark* controls revealed that expression

of these markers alone did not cause obvious phenotypes (Fig. 6A–C, I–K, and data not shown). However, when co-expressed together with *UAS-TBPH-IR* and *UAS-Dcr2* in upper motor neurons, *Gal4*-mediated upper motor neuron-specific *EB1>Dcr2*, *TBPH-IR* RNAi-mediated LOF specifically caused down-regulation of both pre-synaptic *Syt::GFP* and dendritic *DenMark* at day 50 (Fig. 6D–F). To rule out preparation or immunolabeling artifacts, independent replicates of fly brains were similarly processed and analyzed with identical confocal microscopy settings, which established significant reduction of reporter gene expression in pre-synaptic (Fig. 6H) and post-synaptic compartments when compared with age-matched controls (Fig. 6G). Similar analyses were carried out on day 5 and day 40 *Gal4*-mediated upper motor neuron-specific GOF flies, with adult *EB1>Syt::GFP*, *DenMark*, *TBPH* flies showing a down-regulation of both pre-synaptic *Syt::GFP* and dendritic *DenMark* at day 5 and day 40 (Fig. 6L–N) compared with *EB1>Syt::GFP*, *DenMark* controls (Fig. 6I–K). Independent replicates of brains were similarly analyzed and showed a significant reduction of reporter gene expression in pre-synaptic (Fig. 6P) and post-synaptic compartments when compared with age-matched controls (Fig. 6O and data not shown). Together these findings suggest that upper motor neuron-specific TBPH GOF and RNAi LOF affect synaptic integrity; in both cases, phenotypes occur in a progressive and age-related manner, and are associated with severely impaired motor behavior (Figs 3D–H and 5).

### TBPH dysfunction results in age-related and progressive neurodegeneration

Synaptic deficits and subsequent neurodegeneration are considered to be hallmarks of ALS and other neurodegenerative diseases (37,38). We therefore investigated whether *TBPH* LOF and GOF can lead to degenerative cell loss. To visualize and number targeted neurons, we analyzed brains of aged flies that co-express *UAS-mCD8::GFP* with or without either *UAS-TBPH-IR* LOF or *UAS-TBPH* GOF again targeted to *EB1-Gal4* specific upper motor neurons (Fig. 7).

Analysis of *EB1>mCD8::GFP*, *Dcr2*, *TBPH-IR* brains at day 5 and 20 did not reveal any significant differences in neuron numbers; however, by day 40 and 50, we observed a significant reduction of targeted EB neurons (Fig. 7G), showing a worsening of the phenotype over time. For the remaining EB neurons, *mCD8::GFP* labeling revealed misshapen, fragmented and scattered cell bodies when compared with age-matched controls (Figs 7D–F, compare with 7A–C).

number of peristaltic waves per minute compared with controls ( $w^{1118}/+$ , control A; *Elav*/+, control B). (C) TBPH LOF and GOF adults also show poor climbing performance in a startle-induced climbing assay ( $n = 15$ ) compared with controls ( $w^{1118}/+$ , control A; *Elav*/+, control B). (D–H) Video-assisted motion tracking of *TBPH<sup>DD96-/-</sup>* LOF and cell type-specific *EB1>TBPH* GOF targeted to upper motor neurons. (D) Representative walking tracks recorded over 3 min for *TBPH<sup>DD96-/-</sup>* and *EB1>TBPH* flies, together with their respective controls ( $w^{1118}/+$ , control A; *EB1*/+, control C). (E–G) *TBPH<sup>DD96-/-</sup>* LOF and *EB1>TBPH* GOF flies show a reduction in walking activity over time, activity and total distance traveled compared with the respective controls ( $w^{1118}/+$ , control A; *EB1*/+, control C). (H) *TBPH<sup>DD96-/-</sup>* null mutants show reduced walking velocity compared with controls, whereas *EB1*-specific overexpression of TBPH does not affect the mean velocity ( $w^{1118}/+$ , control A; *EB1*/+, control C). (I) *TBPH<sup>DD96-/-</sup>* LOF, *Tub>TBPH-RNAi* downregulation and *ELAV>TBPH* GOF flies display disturbed tripod gait. Left cartoon shows tripod gait with left foreleg (1), right middle leg (2) and left hind leg (3). Control flies ( $w^{1118}$ ) walk in a stereotyped alternating tripod gait pattern. This pattern is disrupted in *TBPH<sup>DD96-/-</sup>* null mutants (*TBPH*-/-), ubiquitous RNAi-mediated TBPH knockdown flies (*Tub>TBPH-RNAi*) and pan-neuronal *Elav-Gal4*-mediated TBPH overexpression flies (*ELAV>TBPH*). Box-plots show median, upper and lower quartiles (box); whiskers contain data  $1.5 \times$  the interquartile range; + indicates a data point within  $3 \times$  the interquartile range (outliers). \*\* $P < 0.01$ ; \*\*\* $P < 0.001$ . Mean and SEM are shown (A, E).



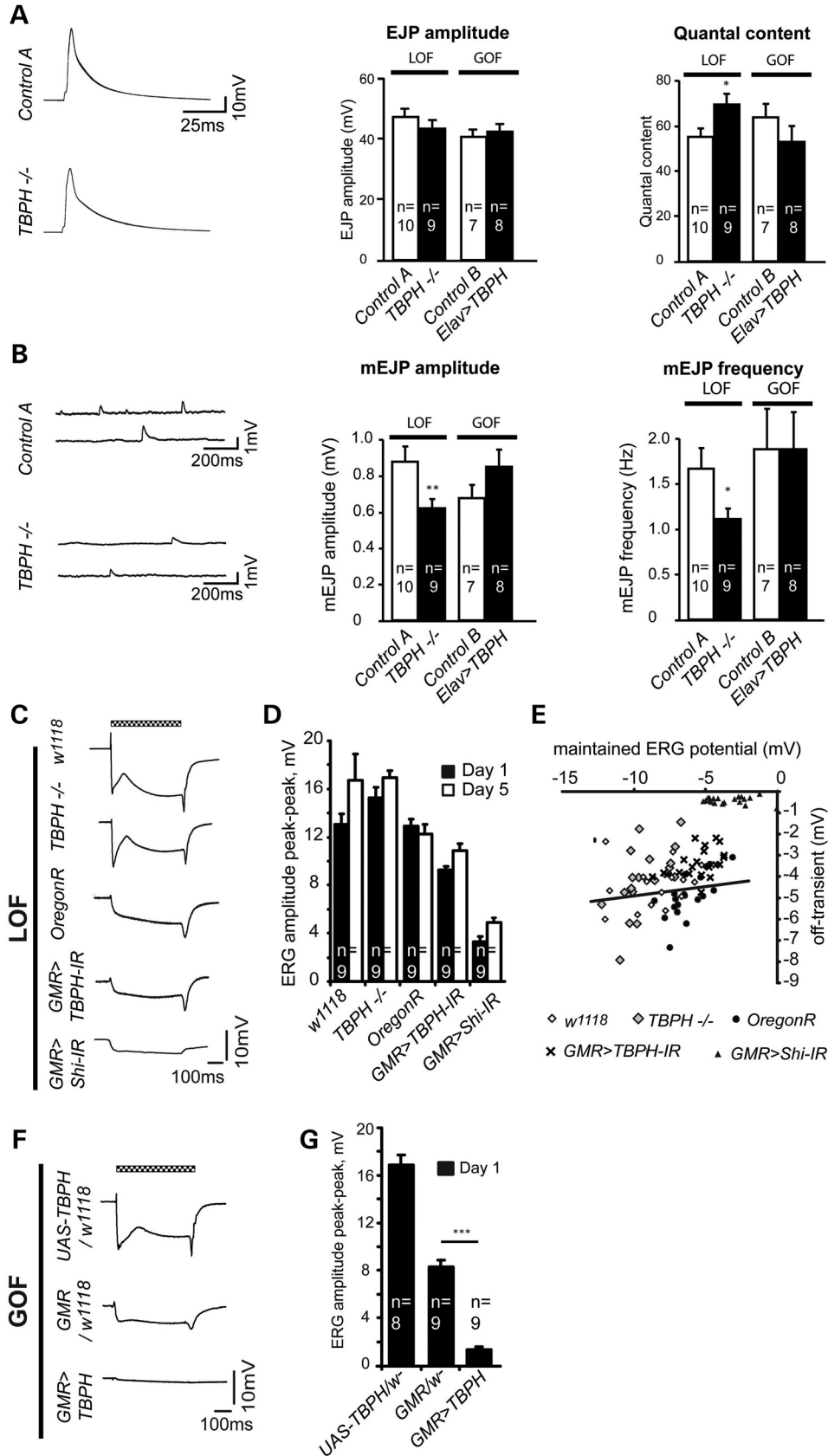


**Figure 4.** TBPH dysfunction affects synaptic efficacy. (A) Representative excitatory junction potential (EJP) traces are shown for LOF. EJP amplitudes for *TBPH<sup>DD96-/-</sup>* LOF and pan-neuronal *ELAV>TBPH* GOF flies are not significantly different from the respective controls (control A, *w<sup>1118</sup>/+* and control B, *Elav/+*), however, quantal content is significantly increased in *TBPH* mutant larvae. (B) Representative traces of spontaneous neurotransmitter release

A comparable but more severe degenerative phenotype was observed in TBPH GOF. Brains of 5-day-old *EB1 > mCD8::GFP, TBPH* flies showed reduced *mCD8::GFP* expression in perikarya as well as axonal extensions and synaptic arborizations of ellipsoid body ring neurons. GFP expression was further reduced by day 40 (Fig. 7K–M, compare with 7H–J) and almost undetectable in day 60 old *EB1 > mCD8::GFP, TBPH* flies when compared with age-matched controls. Analysis of independent replicates of brains of age-matched *EB1 > mCD8::GFP, TBPH* and *EB1 > mCD8::GFP* flies that were similarly processed and analyzed with identical confocal microscopy settings, established significant and progressive, age-related loss of upper motor neurons (Fig. 7N).

To independently confirm age-related and progressive loss of neurons, we studied *pox neuro (poxn)* expression, which is specific to ellipsoid body ring neurons (39). Notably, loss of *poxn*-expressing cells progressed between day 5 and day 40 in *EB1 > mCD8::GFP, TBPH* flies (Supplementary Material, Fig. S13). In addition to the decrease and subsequent loss of *mCD8::GFP* and *poxn* expression, degenerative cell loss was confirmed by the specific and age-related decrease in the number of ellipsoid body ring neurons that expressed excessive amounts of TBPH in *EB1 > mCD8::GFP, TBPH* flies (Supplementary Material, Fig. S4 and data not shown). TUNEL labeling of brains of aged *EB1 > mCD8::GFP, TBPH* flies did not indicate increased apoptotic activity (Supplementary Material, Fig. S14), suggesting that progressive loss of upper motor neurons was not caused by programmed cell death. Together these data suggest that prolonged dysfunction of *Drosophila* TDP-43 causes age-related and progressive neurodegeneration.

### Gain of TBPH does not downregulate or mislocalize endogenous TBPH

The phenotypic similarities between tissue-specific TBPH LOF and GOF may suggest that the observed synaptic deficits, impaired motor behavior and age-related neurodegeneration might be due to a common pathogenic mechanism. Previous *in vitro* and *in vivo* studies indicated that TDP-43 regulates its own expression by a negative feedback loop (17,40,41) that may participate in a feed-forward mechanism whereby cytoplasmic aggregation depletes nuclear TDP-43 function, essentially leading to a loss-of-function phenotype. We tested this hypothesis and over-expressed UAS constructs coding for tagged or untagged full length TBPH (Fig. 8). We utilized *GMR-Gal4* and specifically targeted TBPH GOF to differentiating photoreceptor cells which resulted in a

rough eye phenotype due to photoreceptor cell degeneration (42) (data not shown). Western blot analysis of heads of 1–3-day-old cases and controls identified a 58 kDa band in each condition similar to the control (Fig. 8A). Quantification of independent replicates confirmed that *GMR-Gal4* specific TBPH GOF with C- and/or N-terminal tags did not alter endogenous levels of TBPH expression (Fig. 8B).

We then tested whether *GMR-Gal4* specific TBPH GOF may lead to aggregate formation and/or deplete nuclear expression, hence affecting the function of endogenous TBPH without changing overall TBPH protein levels. Third instar eye imaginal discs were immunolabeled with anti-TBPH and anti-FLAG or anti-HA and counterstained with DAPI to determine potential aggregates and nuclear localization. In none of the cases examined did we detect aggregate formation, nor did we observe loss or alteration of nuclear TBPH expression (Fig. 8C–N and data not shown). We also tested whether *GMR-Gal4*-specific TBPH GOF may result in ubiquitinated TBPH and thus render the endogenous protein non-functional even though expression levels and nuclear localization appeared unaltered. However, immunolabeling with anti-FK2, which recognizes poly-ubiquitination, did not reveal any differences to controls (data not shown). Together these data suggest that gain of *Drosophila* TDP-43 function does not alter its own expression level or localization, although it results in severe synaptic, behavioral and neurodegenerative phenotypes.

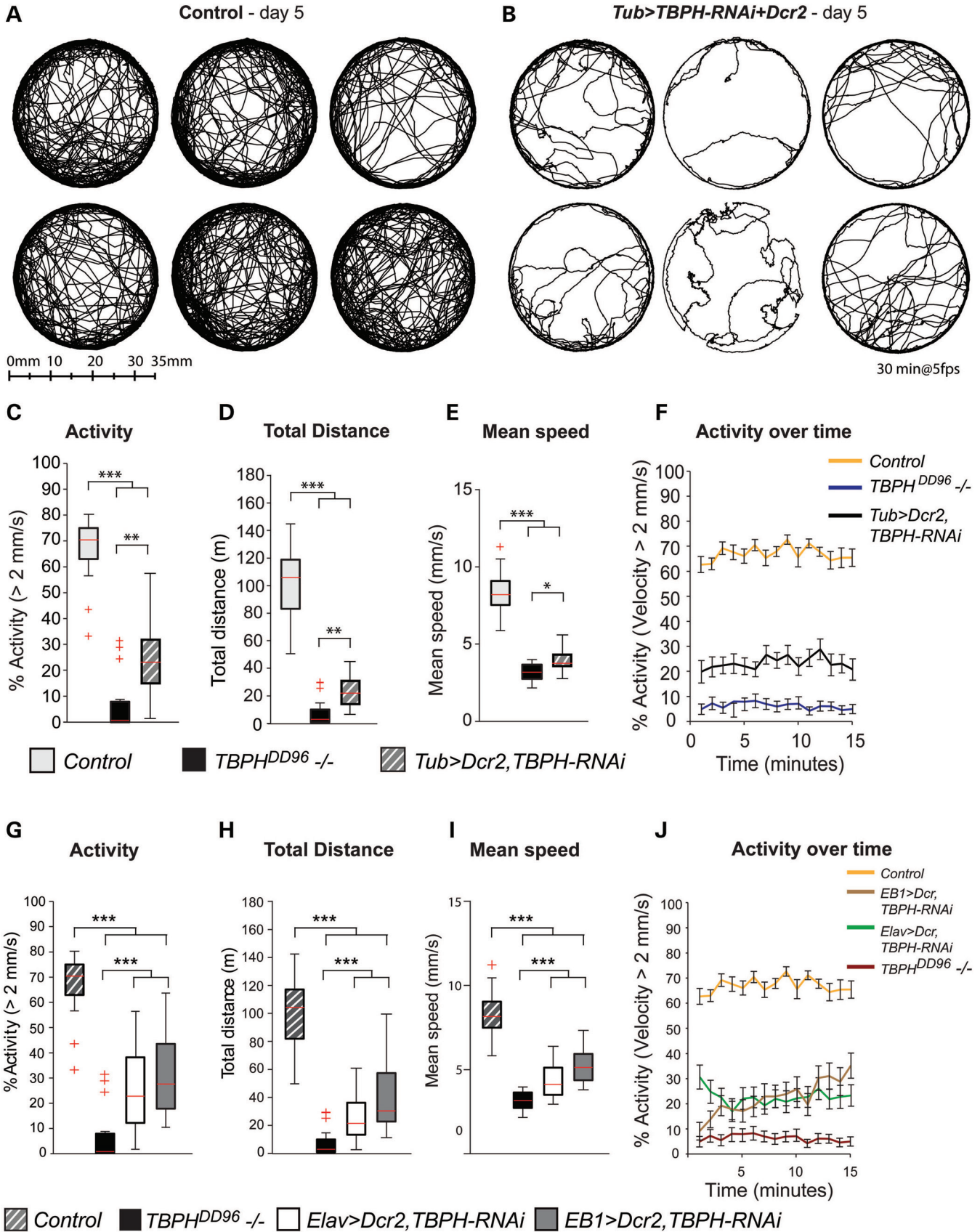
## DISCUSSION

Here we have systematically compared the phenotypic consequences of loss and gain of TDP-43 function in *Drosophila*. Our results demonstrate that deregulation of TBPH affects neuronal function and viability. In either case, deregulated TBPH initiates synaptic deficits and impaired motor behavior, ultimately causing age-related and progressive neurodegeneration. Our findings indicate that common loss-of-function phenotypes underlie TDP-43 dysfunction in *Drosophila*, which has implications for understanding TDP-43-mediated pathogenesis in ALS and FTLD.

### Both loss and gain of TDP-43 trigger disease formation

TDP-43 related ALS and FTLD cases are characterized by both nuclear clearance and the cytoplasmic accumulation of full length, truncated and modified forms of TDP-43 (1). TDP-43 has been shown to autoregulate its own expression (17,41), and its ubiquitylation, phosphorylation, aggregation,

(mEJP) shown for *TBPH<sup>DD96-/-</sup>* LOF. Both the mEJP amplitude and frequency are significantly reduced in *TBPH* mutant larvae. The mEJP is unaffected in *ELAV > TBPH* gain-of-function flies (*w<sup>1118</sup>/+*, control A; *Elav/+*, control B). (C) Representative ERG traces of the indicated TBPH LOF conditions. The white-eyed *TBPH<sup>DD96-/-</sup>* mutants and *w<sup>1118</sup>* flies show a strong, habituating response, steady maintained response and off-transient. The red-eyed OregonR, *GMR > Shibire-IR* and *GMR > TBPH-IR* show a smaller amplitude response; *GMR > Shibire-IR* flies lack on- and off-transients. Chequered bar indicates duration of light pulse. (D) Mean peak–peak amplitude of the ERG from the indicated conditions at day 1 and day 5 timepoints. (E) *TBPH<sup>DD96-/-</sup>* mutant and *GMR > TBPH-IR* have significantly smaller off-transients than the respective eye color-matched controls. The negative *GMR > Shibire-IR* controls, in which synaptic transmission is blocked, show a severely reduced off-transient. The solid line shows the regression line between off-transient and maintained response for wild-type flies. (F) Representative ERG traces of the indicated TBPH GOF conditions. The *UAS-TBPH/+* and *GMR/+* flies show a normal amplitude response, the smaller response seen in the *GMR/+* flies is due to the darker red pigment. *GMR > UAS-TBPH* flies have a very small response, with no off/on transients visible. (G) Mean peak–peak amplitude of the ERG from the indicated GOF conditions at day 1 is significantly decreased in *GMR > TBPH* flies compared with the controls (D, E,  $n = 9$ ; \* $P < 0.05$ , \*\* $P < 0.01$ , \*\*\* $P < 0.001$ ). Mean and SEM are shown (A, B, D, G).





truncation, mislocalization, nuclear clearance and defective autoregulation can contribute either directly or indirectly to disease formation (12). However, no consensus has emerged as to whether loss or toxic gain of TDP-43 function, or both, are causally related to disease onset and progression.

In our study, we systematically compared loss- and gain of *TBPH*, the *Drosophila* homolog of TDP-43, and analyzed their effect on synaptic function and morphology, motor control and age-related neuronal survival. Our results demonstrate that loss of function, RNAi-mediated downregulation and overexpression of wild-type *Drosophila* TDP-43 are sufficient to cause age-related neurodegeneration. In the case of TDP-43 overexpression, we did not detect alterations in expression levels or mislocalization of the endogenous protein; we also found no evidence for ubiquitylation, aggregation, truncation or autoregulation, and based on western blot data, excessive phosphorylation appears unlikely. Our data thus argue that TDP-43 truncation, modification, altered autoregulation or aggregates are not a prerequisite for toxicity and age-related neurodegeneration, which is also supported by data in other model systems (28,41,43–46).

Previous studies showed that TDP-43 can form homodimers (47) and functions in multiprotein/RNA complexes (15,48,49) where multiple TDP-43 molecules are incorporated into each ribonucleoprotein complex (50). These data suggest that equilibrated, physiological levels of TDP-43 and a stoichiometric relationship with ribonucleoprotein complex components are essential for proper biogenesis, spatio-temporal expression and hence, regulation of TDP-43 target genes. Our results establish that deregulation of TDP-43 levels is a core event underlying disease formation, which can be triggered by either decreasing or increasing levels of TDP-43. This suggests that de-regulation of TDP-43 levels, by loss of function, downregulation or overexpression, alters the stoichiometry of participating components and, hence, ribonucleoprotein complex formation required for proper physiological function. In either condition, the net result of de-regulated TDP-43 is impaired physiological function which, when continuing, affects neuronal survival, ultimately causing progressive cell loss. In support of this notion, we determined synaptic deficits as one of the earliest phenotypes of TDP-43 dysfunction.

### Pre-synaptic deficits are early, initiating events of TDP-43-related pathogenesis

In our study, we found that both loss and gain of *Drosophila* TDP-43 result in synaptic deficits and impaired motor behavior, followed by progressive, age-related neurodegeneration.

In contrast to previous reports in *Drosophila* (27,28,29), we did not detect any obvious structural defects at the larval neuromuscular junction or mislocalization of synaptic proteins that might explain the observed behavioral phenotypes. This discrepancy might be attributable to differences in genetic background and/or methods used. Motor terminals are dynamic structures that show developmental and circadian fluctuations in shape and size (51). In our study, we used bona fide *TBPH* null alleles together with genomic rescue, as well as overexpression alleles. Instead of structural defects at the larval NMJ, our experiments reveal that affected flies are characterized by defective synaptic transmission, a phenotype detectable both at the larval NMJ and in the adult. In addition, our tissue-specific RNAi-mediated knock-down experiments identified pre-synaptic, rather than post-synaptic deficits as the earliest detectable phenotypes at the larval NMJ, suggesting that pre-synaptic deficits are initiating events in disease formation.

Our observations therefore allow for the first time the description of a sequence of events whereby TDP-43 dysfunction causes impaired synaptic transmission and motor abnormalities, followed by the subsequent loss of neuronal connections that precede degenerative cell death in an age-related and progressive manner. Such a sequence of events suggests that TDP-43 related pathogenesis progresses from the synapse and axon to the neuronal cell body, thereby resembling affinities to the ‘dying back’ phenomena, a hallmark of several neurodegenerative diseases (37). Comparable events have been, at least to some extent, reported for Wallerian degeneration (52), and recent genetic evidence indicates that neuronal ‘dying back’ underlies an active process of self-destruction distinct from apoptotic cell death (53). A ‘dying back’ process also characterizes human ALS patients and mouse superoxide dismutase 1 (SOD1) models of ALS (38,54). Like TDP-43 inclusions, SOD1 mutations are commonly identified in familial ALS (55). Although further, conclusive experiments are required, it is tempting to speculate that TDP-43 might not only regulate RNAs related to synaptic function (15,17), but potentially also negatively regulates the transcription or translation of target genes involved in the active self-destruction of neuronal connections.

### TDP-43 dysfunction results in loss-of-function phenotypes

In addition to similarities between loss and gain of function phenotypes, we also observed phenotypic differences, including electrophysiology at the larval NMJ but also at the level of synaptic integrity and neurodegeneration in adult brain, where

**Figure 5.** Similar to *TBPH* mutants, cell-type specific knockdown of *TBPH* leads to impaired motor behavior. Gal4-mediated UAS-*TBPH*-RNAi knockdown targeted either ubiquitously (*Tub-Gal4*) or to all neurons (*Elav-Gal4*), or targeted to upper motor neurons (*EB1-Gal4*). RNAi efficiency was enhanced by co-expressing *UAS-Dcr2*. (A–J) Motor behavior analysis using video assisted open-field motion tracking. (A) Representative walking tracks recorded over 30 min for 5-day-old *Tub>Dcr2, TBPH-RNAi* flies and heterozygous *Dcr2, TBPH-RNAi* controls. (C–F) Tracking analyses reveal that, comparable to *TBPH<sup>DD96-/-</sup>* mutants, *Tub>Dcr2, TBPH-RNAi* flies have a significantly reduced average activity, total distance travelled, mean speed and activity over time when compared with heterozygous *Dcr2, TBPH-RNAi* controls. (G–J) *Dcr2, TBPH-RNAi* expression was activated by either the pan-neuronal ELAV-Gal4 driver, or the EB1-Gal4 driver (*ELAV>Dcr2, TBPH-RNAi* or *EB1>Dcr2, TBPH-RNAi*, respectively). Tracking analyses reveal that, comparable to *TBPH<sup>DD96-/-</sup>* mutants, the walking activity, total distance travelled, mean speed and activity over time of 5-day-old *ELAV>Dcr2, TBPH-RNAi* and *EB1>Dcr2, TBPH-RNAi* flies is significantly reduced when compared with that of the control (heterozygous *Dcr2, TBPH-RNAi*). Box-plots show median, upper and lower quartiles (box); whiskers contain data 1.5× the interquartile range; + indicates a data point within 3× the interquartile range (outliers). (*n* = 24; \**P* < 0.05, \*\**P* < 0.01, \*\*\**P* < 0.001). Mean and SEM are shown (F, J).

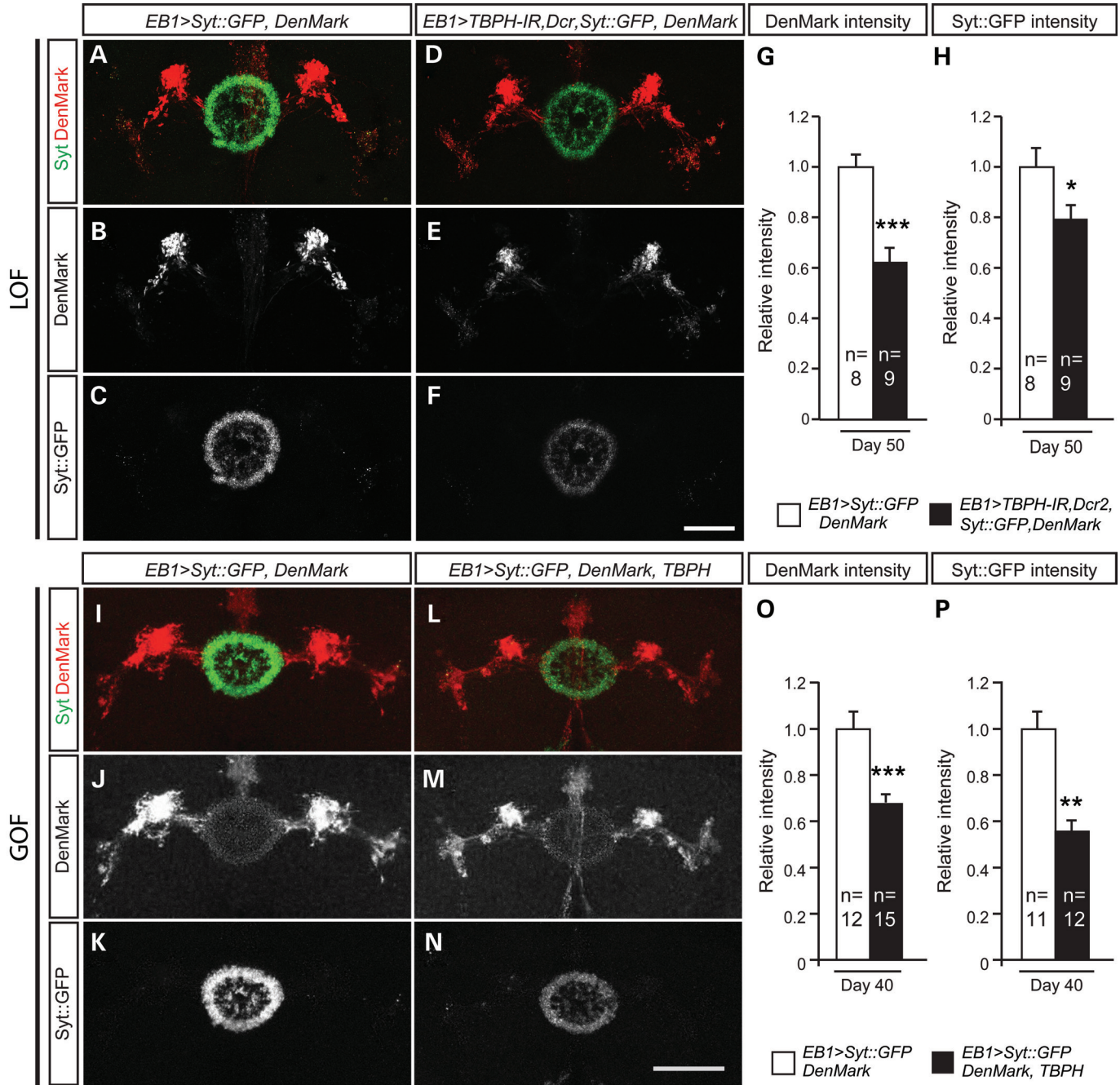


**Figure 6.** Both cell type-specific TBPH LOF and GOF cause trans-synaptic defects. (A) Expression of pre-synaptic marker *Syt::GFP* (green) and dendritic marker DenMark (red) in upper motor neurons of the adult central brain of 50-day-old flies using the ellipsoid body neuron-specific *EB1-Gal4* driver (*EB1>Syt::GFP, DenMark*). *Syt::GFP* (green) expression is seen in the pre-synaptic region, whereas *DenMark* visualizes post-synaptic dendritic compartment. *DenMark* signal and *Syt::GFP* are indicated in single panels (B and C, respectively). (D–F) Driving TBPH-RNAi in EB1 neurons leads to downregulation of *DenMark* (E) and *Syt::GFP* (F). (G) *DenMark* signal is significantly reduced in TBPH LOF (*EB1>Syt::GFP, DenMark, TBPH-IR*). (H) TBPH knockdown significantly downregulates *Syt::GFP*. (I–K) *DenMark* (J) and *Syt::GFP* (K) expression in EB1 neurons of 40-day-old flies. (L and M) TBPH overexpression in EB1 neurons leads to downregulation of *DenMark* (M) and *Syt::GFP* (N). (O) *DenMark* signal is significantly reduced in TBPH GOF (*EB1>Syt::GFP, DenMark, TBPH*). (P) TBPH overexpression significantly downregulates *Syt::GFP*. \* $P < 0.05$ , \*\* $P < 0.01$ , \*\*\* $P < 0.001$ . Mean and SEM are shown. Scale bar: 50  $\mu$ m.

GOF typically caused more severe phenotypes than LOF. While some of these differences might be attributable to differing efficiencies of UAS/Gal4-mediated LOF and GOF, or a possible gain of toxic function, it is striking that both conditions lead to

comparable, detrimental phenotypes with similar endpoint: age-related and progressive neurodegeneration.

It should be emphasized, however, that the similar phenotypic outcomes of loss and gain of *Drosophila* TDP-43



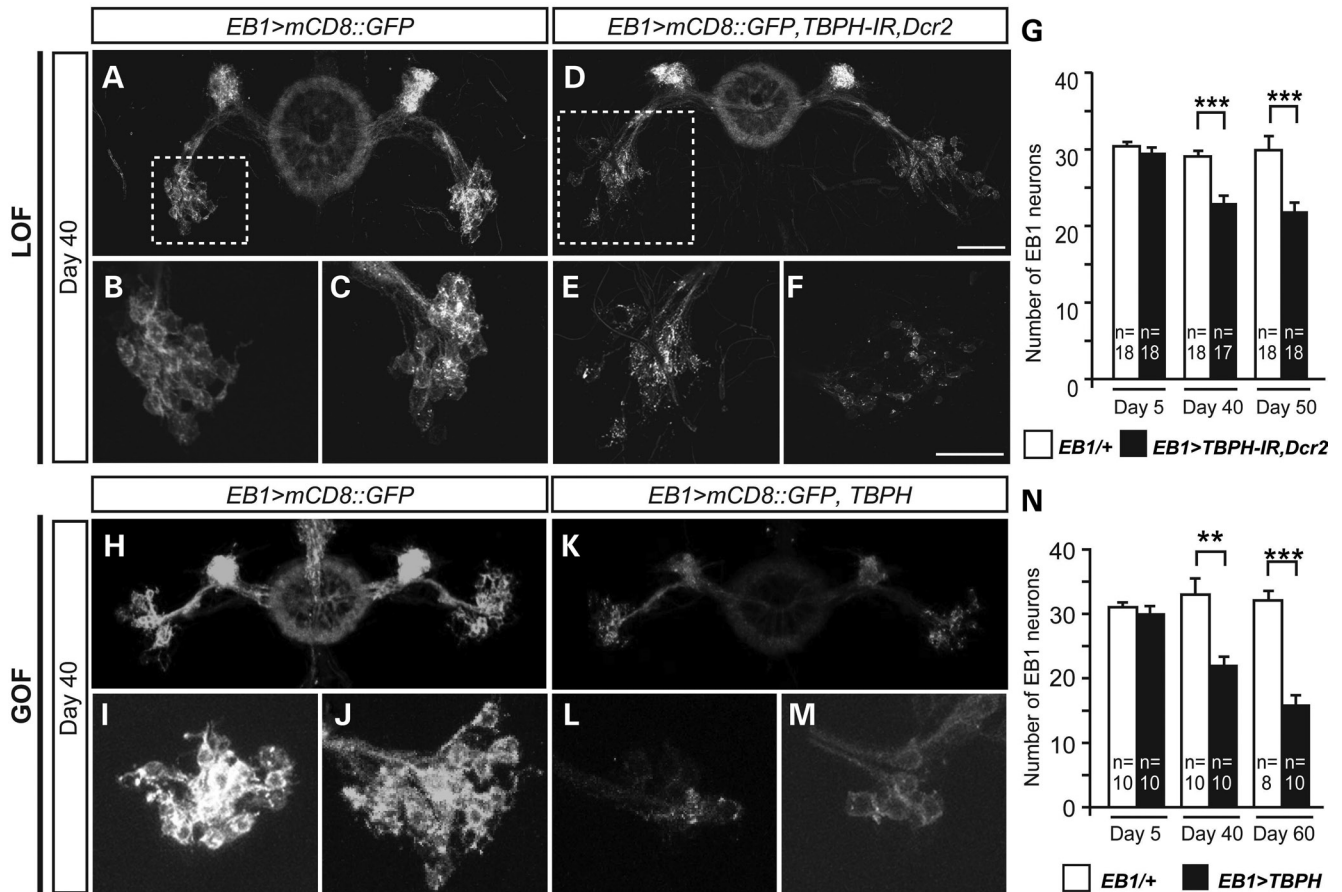


**Figure 7.** Upper motor neuron-specific RNAi-mediated downregulation and gain of TBPH causes loss of neuronal connections and age-related neurodegeneration. (A–C) Control flies with *mCD8::GFP* overexpression in upper motor neurons at day 40 (B, enlargement of dashed box in A; C, additional example). (D–F) TBPH LOF flies (*EB1>mCD8::GFP, Dcr2, TBPH-IR*) with TBPH-RNAi targeted to upper motor neurons at day 40. The GFP expression in the ellipsoid body structure does not diminish in the aged brain, however, dispersed cells with fragmented and granular GFP expression are detectable (E, enlargement of dashed box in D; F, additional example). (G) Quantification of EB1 neuron cell number (GFP positive) in control and TBPH LOF flies at day 5, 40 and 50. A significant decrease in neuron number is observed in aged TBPH LOF flies. (H–J) Control flies with *mCD8::GFP* overexpression in EB1 ring neurons at day 40 (I–J, enlarged example of cell bodies). (K–M) TBPH and *mCD8::GFP* overexpression in upper motor neurons leads to an age-related reduction in *mCD8::GFP* expression (L–M, enlarged example of cell bodies). (N) Quantification of EB1 cell numbers (GFP positive) in control and TBPH GOF flies at day 5, 40 and 60. A significant decrease in neuron number is observed over time in TBPH GOF flies. \*\* $P < 0.01$ , \*\*\* $P < 0.001$ . Mean and SEM are indicated. Scale bar: 50  $\mu$ m.

function, including age-related neurodegeneration, do not necessarily implicate similar mechanisms related to TDP-43 mediated pathogenesis. It is conceivable but remains to be shown that loss, downregulation or gain of TDP-43 function could trigger distinct pathogenic mechanisms that all converge on a functional node which when defective initiates disease formation. Previous studies suggest that such a functional node is likely the stoichiometric activity of TDP-43 in ribonucleoprotein complexes that are essential for the regulation and correct processing of multiple target genes, including those related to synaptic function (15,17). This model is consistent with familial cases of ALS and FTLN, where TDP-43 is predominantly mutated in the C-terminal, prion-like domain (5–8) that regulates tissue-specific gene expression, transcriptional repression and alternative splicing, and is essential for binding to ribonucleoproteins involved in microRNA and mRNA biogenesis, as well as RNA turnover (9,10,12,13). According to this model, C-terminal, but also RRM mutations

may hinder the participation of TDP-43 in ribonucleoprotein complex formation and hence, their function, leading to physiological deficits and eventually neurodegeneration.

In summary, our findings demonstrate that both loss and gain of TDP-43 function result in functional deficits whereby impaired synaptic transmission and defective motor behavior precede progressive deconstruction of neuronal connections, ultimately causing age-related neurodegeneration. Our data therefore provide *in vivo* evidence for common loss-of-function phenotypes underlying TDP-43 dysfunction that likely also characterize TDP-43-mediated ALS and FTLN.

## MATERIALS AND METHODS

### Fly stocks

Fly stocks were maintained at 25°C on standard cornmeal food, unless for aging experiments where aged flies



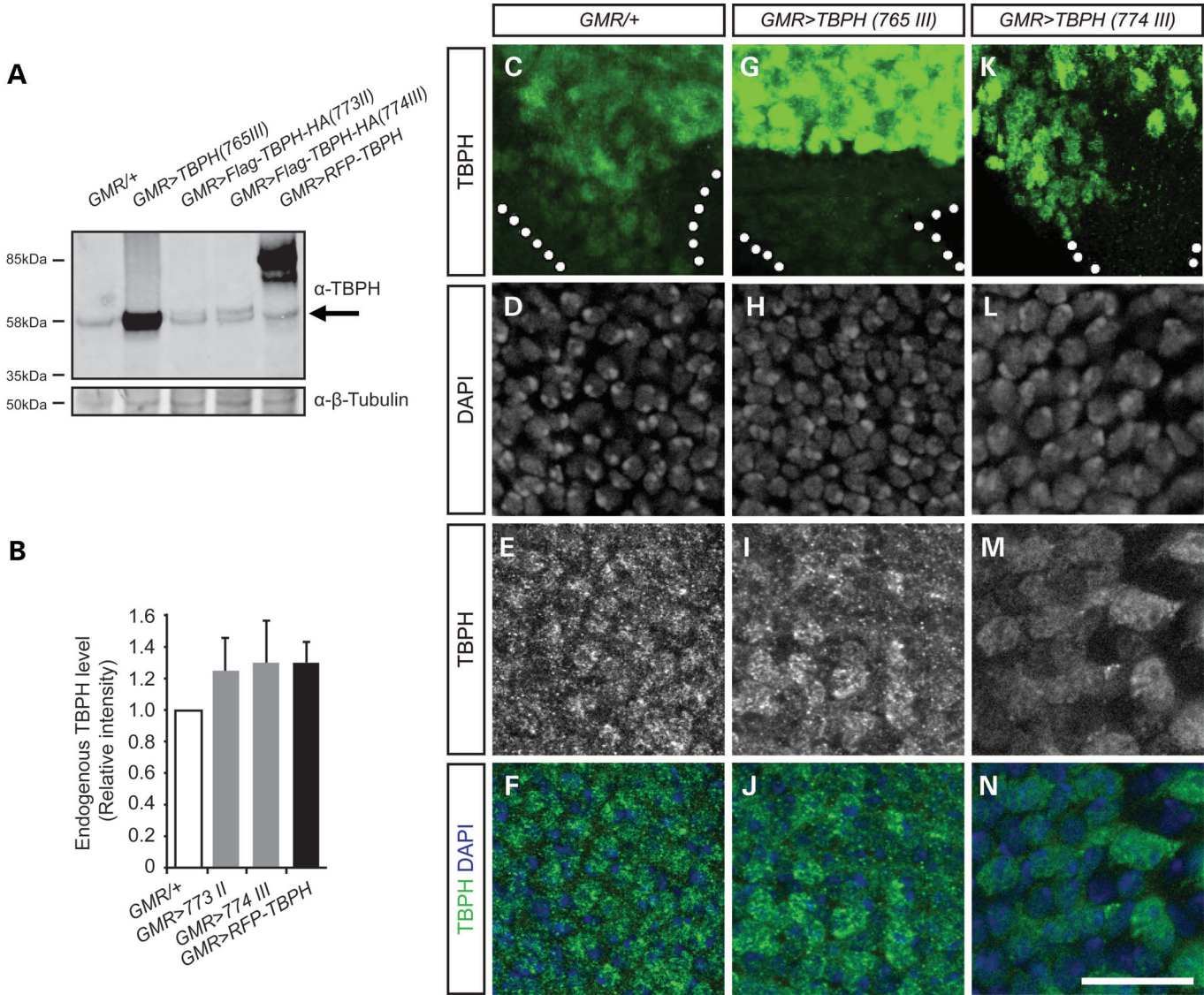


**Figure 8.** GMR-Gal4-mediated gain of TBPH does not downregulate or mislocalize endogenous TBPH. (A) Western blot analysis of GMR-Gal4-driven untagged (58 kDa) or tagged UAS-TBPH (Flag-TBPH-HA, 60 kDa; RFP-TBPH, 85 kDa). Levels of endogenous TBPH (arrow at 58 kDa) are unaffected in day 1-3 flies overexpressing either form of TBPH. (B) Quantification of endogenous TBPH shows no alteration in TBPH protein levels. Endogenous TBPH signal intensities were normalized against  $\beta$ -Tubulin. Mean and SEM are indicated. (C, G, K) Third instar eye imaginal discs immunolabeled with anti-TBPH does not reveal TBPH-positive aggregates in cell bodies nor in the optic stalk (dotted area). (D-F, H-J, L-N) Third instar eye imaginal discs immunolabeled with anti-TBPH and DAPI identifies that nuclear expression of endogenous TBPH is maintained in gain of TBPH. Note that signal intensity in I, J, M and N is adjusted for overexpressed TBPH to avoid saturation of the signal. Scale bar: 10  $\mu$ m.

were maintained on 15% sugar/yeast medium (23). The following strains were used: *Oregon R* (wild-type); *w<sup>1118</sup>*; *w*; *TBPH<sup>null</sup>/CyO,GFP*; + (26) *Df(2R)106/SM5*; *w*; +; *Elav-Gal4*; *GMR-Gal4*; and *Tub-Gal4*; *UAS-mCD8::GFP* (56); *UAS-Dcr2*; *UAS-Shibire-RNAi* (Bloomington Stock Centre); p{Gawb}C57 (BG57, ref. 34); *EB1-Gal4* (57); *UAS-DenMark*, *UAS-Syt::GFP* (36); *UAS-RFP-TBPH* (58).

### Transgenic constructs

The *TBPH* gene was amplified by PCR from cDNA clone GH09868 (DGRC). PCR primers to amplify TBPH in pUAST vector are forward primer: 5'-GGAGATCTATGGA

TTTCGTTCAAGTGTCCG-3'; reverse primer: 5'-GGCTCG AGTTAAAGAAAGTTTGACTTCTCCGC-3'.

Primers used to generate Flag-TBPH-HA are: forward primer: 5'-GGAGATCTATGACTACAAGGACGACGATGACAAG GATTCGTTCAAGTGTCCG-3'; reverse primer: 5'-GGCTC GAGTTAGGCATAGTCTGGGACGTCATATGGATAAAG AAAGTTTGACTTCTCCGC-3'.

*Bgl*II and *Xho*I sites were used to insert TBPH into pUAST vector. DNA sequence was confirmed by sequencing. The *UAS-TBPH<sup>Y4765</sup>* line was used for all behavioral, electrophysiology and immunohistochemistry experiments. To specifically knockdown TBPH, the target region was chosen by E-RNAi web service (59). TBPH RNAi construction was carried out

as previously described (33). PCR primers with *EcoRI* (forward) and *XbaI* (reverse) sites were designed to subclone TBPH RNAi construct into pMF3 vector (33).

*TBPH-RNAi*: forward primer: 5'-GGGAATTCCACTCATA CCACCCACAGGG-3'; reverse primer: 5'-GGTCTAGA GTTATGCGGCTGGTTCATTC-3'.

Insertion of RNAi construct was confirmed by restriction enzyme digestion and sequencing. Plasmid injection and generation of transgenic flies were performed by BestGene Inc (CA, USA).

To generate a TBPH genomic rescue construct, we used TBPH genomic DNA from pacman bac library (CH322-116J04, bacpac.chori.org) covering position 19751906–19744713 on the second chromosome, which encodes the entire TBPH coding sequence. *TBPH<sup>genomic</sup>* was integrated into the pUC 3GLA plasmid (gift from Matthias Soller) by recombination. *TBPH<sup>genomic</sup>* in pUC 3GLA was used to generate transgenic flies by site-specific integration into the attp86Fb fly strain (60) and flies harboring *TBPH<sup>genomic</sup>* pUC 3GLA were selected by compound eye-specific GFP expression.

### P-element-mediated mutagenesis

The *TBPH<sup>DD96</sup>* and *TBPH<sup>DD100</sup>* null alleles were generated by imprecise excision of the EY10530 P-element, which is inserted in the promoter region of the *TBPH* locus. It was mobilized using HoP1  $\Delta$ 2-3 transposase (gift from Iris Salecker). Four hundred and fifty excision lines were established from individual events and genomic deletions within the TBPH locus were identified by PCR and confirmed as protein null by western blot. *TBPH<sup>DD96</sup>* and *TBPH<sup>DD100</sup>* breakpoints are 19750093...19747817 and 19750093...19747925, respectively. The primers used to confirm the presence of neighboring gene CG4585 were: forward primer: 5'-CTGAGCATCTTCTGCGAC-3'; reverse primer: 5'-GAAATTAGCTCGCCATGG-3'.

Breakpoints and P-element insertion sites were sequenced using the following primers: *TBPH<sup>DD100</sup>*, forward primer: 5'-TTCCATGGCGAGCTAATT-3'; reverse primer: 5'-GTG TCCAGGTTGCGTACTT-3' *TBPH<sup>DD96</sup>* forward primer: 5'-CGAGTTGCCGCGTAAT-3'; reverse primer: 5'-CCTT TCACTCGCACTTAT-3'. Sequencing was carried out at MWG Eurofins.

### Generation of TBPH antibody

The anti-TBPH antibody was generated by injecting two rabbits with peptide sequences PQGNHMNPNRNGHHR, corresponding to residues 291–305 and QSSGSQNAAEKSNFL, residues 517–531. Immunization was carried out by Eurogentec.

### Immunohistochemistry

Adult and larval CNS dissection was carried out as previously described (23). Larval NMJ dissections were carried out according to established protocol (61). Primary antibodies used were: mouse anti-Repo (1:20); rat anti-Elav (1:30);

mouse anti-Futsch (1:50); mouse 3C11 (1:100); mouse anti-synaptotagmin (1:25); mouse anti-FasII (1:10); mouse NC82 (anti-bruchpilot) (1:100) and mouse anti-Neuroglian (1:4) all obtained from the Developmental Studies Hybridoma Bank (DSHB) under the auspices of the NICHD and maintained by The University of Iowa; rabbit anti-TBPH antibody (1:3000); rabbit anti-Poxn (1:100; Adachi, Ludlow & Hirth, unpublished); mouse anti-polyubiquitin (FK2, 1:200; ENZO); rabbit anti-FLAG (1:500; Cell Signaling Tech); mouse anti-HA (1:40; Roche); goat anti-HRPCy3 (1:100; Stra-tech), 488-Phalloidin (1:1000; Invitrogen). Secondary antibodies were Alexa fluor 488, 568 and 647 (each 1:150; Invitrogen).

### Image acquisition and analysis

Images were obtained either with Motic BA400 or Leica TCS SP5 confocal microscope with Leica Application Suite Advanced Fluorescence (LAS AF) version 2.0.2 software. For confocal images, channels were scanned sequentially. For comparative images, the same microscope settings were used for the control and experimental genotypes. For Figs 6 and 7, confocal z-stacks were rendered as 3-D projections. Signal quantification of digital images was carried out using Fiji (FIJI). Significance of GFP and FasII signal intensity was calculated using unpaired Student's *t*-test. Equal variance assumptions were based on Levene's test for equality of variance.

### NMJ bouton count

Early L1 larvae were picked from 4 h egg collection plates (fruit agar) and placed on cornmeal food. At wandering L3, larvae were dissected according to established protocol (61). All preparations were dissected within a 1.5 h window to avoid differences in circadian rhythm effect on bouton number. Z-stacks were taken of the MN6/7-Ib motor neurons innervating muscle group 6/7 in segment A3. Boutons were counted by hand and the number of NC82 puncta were analyzed using the ITCN plug-in for ImageJ.

### Terminal deoxynucleotidyl transferase dUTP nick end labeling (TUNEL) assay

Tissues of interest were fixed in 4% formaldehyde and subsequently permeabilized in 100 mM Citrate/0.1% Triton X-100 for 30 min at 65°C. Tissues were briefly washed with 0.5% Triton-X 100 in PBS and rinsed twice with TUNEL assay buffer (In Situ Cell Death Detection Kit; Roche). After incubating for 90 min at 37°C, TdT enzyme was added and further incubated for 3 h at 37°C. For positive control, freshly dissected tissue was soaked in 2N HCl for 30 min to induce apoptosis.

### Western blots

Fly tissue was lysed in RIPA buffer (150 mM NaCl, 1% NP-40, 5 mM EDTA, 0.5% sodium, deoxycholate and 0.1% SDS, 50 mM Tris, pH8.0) containing complete proteinase inhibitor (Roche) and phosstop phosphatase inhibitor (Roche).



Samples were centrifuged to take the RIPA-soluble fraction. SDS-PAGE was run in 8% SDS gel. Rabbit anti-TBPH antibody was used at 1:2000–3000 and anti- $\beta$ -Tub (DSHB) was used at 1:300. Secondary antibodies were IRDye 800 conjugated goat anti-rabbit (1:10000, Rockland Immunochemicals) and Alexa Fluor 680 goat anti-mouse (1:10000, Invitrogen). Membrane images were acquired using Odyssey.

### Reverse transcriptase PCR

RNA was extracted by homogenizing whole flies in Trizol, adding chloroform, incubating on ice for 15 min, followed by centrifugation at 16 000g at 4°C. The upper phase was added to isopropanol and incubated and spun as before. The pellet was washed in 70% ethanol and dissolved in nuclease-free H<sub>2</sub>O. RNA purity was measured using a Nanodrop. DNase treatment was carried out according to manufacturer's instructions (Ambion). cDNA was generated by mixing 1  $\mu$ g RNA and random hexamers, heating to 70°C and adding 5  $\times$  M-MLV reaction buffer, M-MLV-RT, RNasin and dNTPs according to manufacturer's instructions (Ambion). Samples were incubated at 37°C for 1 h and 70°C for 15 min. PCR products were run on 1% agarose gel. The primers used were as follows; *TBPH*: forward primer: 5'-ATCTTGATGGCTCAGAACG-3', reverse primer: 5'-GT CGGTCTTTATTCCGTTGG-3' *RPL32*: forward primer: 5'-CGCCGCTTCAAGGGACAGTATC-3', reverse primer: 5'-CGACAATCTCCTTGCGCTTCTT-3'.

### Footprint/gait analysis

Flies were briefly anaesthetized with CO<sub>2</sub> and one-third of the wings were removed to prevent escape. Flies were left to recover in a petri dish for 10–15 min before being tapped onto a soot-covered glass microscope slide (slides were held over a candle flame until covered in an even coating of soot). Footprints were visualized by lighting the slide from below and images were captured with a Q-capture camera.

### Startle-induced negative geotaxis

Flies' climbing ability was assayed as described earlier (23). Equal variance assumptions were based on Levene's test for equality of variance.

### Eclosion analysis

Embryos were collected on fruit agar plates in 5 h batches and left in a 25°C incubator until larvae had hatched. Fifty first instar larvae were placed in a vial and a tally made of all fully eclosed adult flies, mean values were calculated and plotted as a percentage of total number of larvae picked. Significance was calculated using unpaired *t*-test. This was carried out in triplicate for each genotype.

### Larval motility

Thirty wandering third instar larvae were individually placed on a fruit agar plate and allowed to recover for 30 s. The number of peristaltic waves, travelling in either direction,

was scored over 1 min. Significance was calculated using unpaired *t*-test (two-tailed). Equal variance assumptions were based on Levene's test for equality of variance.

### Video-assisted motion tracking

Tracking arenas were modified six-well tissue culture plates (35 mm diameter wells) filled with silicon rubber (Sylguard) to leave a 3 mm space so that flies could walk freely but not hop or fly. 18–24 flies were briefly anaesthetized with CO<sub>2</sub>, placed in separate arenas and left to recover at 25°C for 45 min before being placed above an array of white LEDs within a temperature-controlled incubator. Tracking was carried out at 25°C. A black and white CCD camera (Hitachi, MP-M1A) positioned above the arenas was connected to a PC via an analog capture card (Integral Technologies, Flashbus MV Lite). Recordings were carried out during the same time slot. Recorded videos were converted to fly movie format using the motmot package (62) and loaded into Ctrax software (63) to analyze the positions of the flies throughout the video. Position data for the 30 min file was exported as a Matlab-compatible (Mathworks) matrix file. Errors in the tracking were fixed using Matlab (Mathworks) as well as FixErrors GUI (63), which is described in further detail at <http://ctrax.sourceforge.net/fixerrors.html>. Fixed trajectories were analyzed in Matlab using custom scripts (written by D.M.H). This analysis determined the mean velocity, mean activity, activity over time and mean cumulative distance traveled by the population of flies in the arena. Activity was defined as movement per frame above a velocity of 2 mm/s. Average activity was the percentage of frames where the fly was active (>2 mm/s velocity). Mean velocity was the average of velocities in each frame of the recording only when the fly was active. Box-plots were generated in Matlab where the boxes show median, upper and lower quartiles; whiskers contain data 1.5 $\times$  the interquartile range; + indicates a data point within 3 $\times$  the interquartile range. Significance was calculated using the Mann–Whitney *U*-test with a Bonferroni correction to account for multiple comparisons.

### Escape response

The amplitude of the escape response was carried out as previously described (64). In summary, anaesthetized flies were fixed to a tungsten pin on the end of a cocktail stick using glue gum. The pin was placed so that it covered the thorax. Flies were left to recover for 20 min before being mounted over the flexible ergometer and lowered gently until the flies reached out and place their legs on the jump platform, bringing it up to a resting position. A stimulating electrode was placed in the eye and one in the cervical connective to stimulate the Giant Fiber System. A supra-threshold 0.8 mV was applied and as the flies jumped, the amount of beam displacement was measured.

### Electrophysiology

Wandering third instar larvae were dissected in HL3 buffer (65) containing 1.8 mM CaCl<sub>2</sub>. Nerves innervating the body muscle walls were cut near the ventral ganglion and stimulated



using a suction electrode and isolated pulse stimulator Digitimer DS2A (constant current modification), with a current double that needed to initiate a compound response. All recordings for TBPH LOF/GOF and appropriate controls were made intracellularly in muscle 6, abdominal segment 3, at ambient room temperature using microelectrodes filled with 3 M KCl that had tip resistances of 5–10 M $\Omega$ . In 1.8 mm extracellular Ca<sup>2+</sup> resting membrane potentials were  $-61.1 \pm 1.0$  mV ( $n = 10$ ) and  $-55.8 \pm 2.5$  mV ( $n = 9$ ,  $P < 0.05$ ) and input resistances were  $10.1 \pm 0.7$  M $\Omega$  ( $n = 10$ ) and  $9.6 \pm 0.4$  M $\Omega$  ( $n = 9$ ,  $P > 0.05$ ) for *w<sup>1118</sup>* and TBPH<sup>-/-</sup> larvae, respectively. Resting membrane potentials were  $-54.1 \pm 1.4$  mV ( $n = 7$ ) and  $-52.0 \pm 1.5$  mV ( $n = 8$ ,  $P = 0.0018$ ) and input resistances were  $5.9 \pm 0.2$  M $\Omega$  ( $n = 7$ ) and  $6.4 \pm 0.3$  M $\Omega$  ( $n = 8$ ,  $P < 0.05$ ) for ELAV/+ and ELAV>TBPH, respectively. Data, filtered at 1 kHz and digitized at 10 kHz, were acquired using an Axopatch 200B amplifier and a Digidata 1320A data acquisition board (Molecular Devices Data) were acquired using pClamp8.02 (Molecular Devices) and analyzed with Clampfit8.02 (Molecular Devices) or MiniAnalysis (Synaptosoft). EJP amplitude histograms were constructed by averaging 50 separate events stimulated at 0.2 Hz from an individual muscle cell and then calculating the mean response from at least six larvae per line. Spontaneous release events were recorded for 120 s without any electrical stimulation. All events were analyzed and mean mEJP amplitudes from individual larvae were averaged to generate the histograms. To obtain the frequency of spontaneous release events the number of events for each recording was divided by 120 and then averaged to generate histograms. Significance was calculated using unpaired Students *t*-test (two-tailed).

### Electroretinograms

Female flies were aspirated into a pooter, and then gently blown into a truncated pipette tip. They were restrained with nail varnish (Creative Nail Design). No anaesthesia was used. Blunt glass pipettes, filled with simple *Drosophila* saline (130 mM NaCl, 4.7 mM KCl, 1.9 mM CaCl<sub>2</sub> (66)) were used as recording electrodes, placing one tip centrally on the surface of the eye and the other in the mouthparts. Flies were adapted to the dark for 2 min and then presented with a standard blue light stimulus from three Kingbright, KAF-5060PBESEEVGC light-emitting diodes (maximum emission wavelength 465 nm) situated 6 cm away from the eye. Light pulses were monitored with a BPX65 photodiode (Centronics) next to the head of the fly. In the dark, the photodiode current was 0.5 nA; during the stimuli 400 nA. Each fly was tested with at least three blue light stimuli, >10 s apart. Their responses were captured using DasyLab software (measX, Mönchengladbach, Stuttgart) and the average waveform calculated. At least nine flies of each genotype were tested at each timepoint. Significance was calculated using Bonferroni *post hoc* analysis.

### Statistical analysis

Statistical analysis was carried out as previously described (24); for details of the statistical tests used, see Supplementary Material, Table S1.

## SUPPLEMENTARY MATERIAL

Supplementary Material is available at *HMG* online.

## ACKNOWLEDGEMENTS

We thank B. Hassan, T. Lee, I. Salecker, A. Voigt, D.C. Zarnescu, the Bloomington Stock Centre, the Vienna Drosophila RNAi Centre and the Developmental Studies Hybridoma Bank at the University of Iowa for stocks and reagents.

*Conflict of Interest statement.* None declared.

## FUNDING

This work was supported by the UK Medical Research Council (G-0802208 to I.M.R. and G-070149 to F.H.), the Royal Society (Hirth/2007/R2 to F.H.), the Motor Neurone Disease Association (Hirth/Oct07/6233 to F.H., A.A.-C., C.E.S. and Hirth/Mar12/6085 to F.H. and C.E.S.), Parkinson's UK (G-0714 to F.H.), Alzheimer's Research UK (ARUK-PhD2012-18 to F.H.) and the Fondation Thierry Latran (2/2011/DrosAls to F.H.). Funding to pay the Open Access publication charges for this article was provided by the UK Medical Research Council and the Fondation Thierry Latran.

## REFERENCES

1. Neumann, M., Sampathu, D.M., Kwong, L.K., Truax, A.C., Micsenyi, M.C., Chou, T.T., Bruce, J., Schuck, T., Grossman, M., Clark, C.M. *et al.* (2006) Ubiquitinated TDP-43 in frontotemporal lobar degeneration and amyotrophic lateral sclerosis. *Science*, **314**, 130–133.
2. Arai, T., Hasegawa, M., Akiyama, H., Ikeda, K., Nonaka, T., Mori, H., Mann, D., Tsuchiya, K., Yoshida, M., Hashizume, Y. *et al.* (2006) TDP-43 is a component of ubiquitin-positive tau-negative inclusions in frontotemporal lobar degeneration and amyotrophic lateral sclerosis. *Biochem. Biophys. Res. Commun.*, **351**, 602–611.
3. Forman, M.S., Trojanowski, J.Q. and Lee, V.M. (2007) TDP-43: a novel neurodegenerative proteinopathy. *Curr. Opin. Neurobiol.*, **17**, 548–555.
4. Chen-Plotkin, A.S., Trojanowski, J.Q. and Lee, V.M. (2010) TAR DNA-binding protein 43 in neurodegenerative disease. *Nat. Rev. Neurol.*, **6**, 211–220.
5. Sreedharan, J., Blair, I.P., Tripathi, V.B., Hu, X., Vance, C., Rogelj, B., Ackerley, S., Durnall, J.C., Williams, K.L., Buratti, E. *et al.* (2008) TDP-43 mutations in familial and sporadic amyotrophic lateral sclerosis. *Science*, **319**, 1668–1672.
6. Gitcho, M.A., Baloh, R.H., Chakraverty, S., Mayo, K., Norton, J.B., Levitch, D., Hatanpaa, K.J., White, C.L. 3rd, Bigio, E.H., Caselli, R. *et al.* (2008) TDP-43 A315T mutation in familial motor neuron disease. *Ann. Neurol.*, **63**, 535–538.
7. Kabashi, E., Valdmanis, P.N., Dion, P., Spiegelman, D., McConkey, B.J., Vande Velde, C., Bouchard, J.P., Lacomblez, L., Pochigaeva, K., Salachas, F. *et al.* (2008) TARDBP mutations in individuals with sporadic and familial amyotrophic lateral sclerosis. *Nat. Genet.*, **40**, 572–574.
8. Yokoseki, A., Shiga, A., Tan, C.F., Tagawa, A., Kaneko, H., Koyama, A., Eguchi, H., Tsujino, A., Ikeuchi, T., Kakita, A. *et al.* (2008) TDP-43 mutation in familial amyotrophic lateral sclerosis. *Ann. Neurol.*, **63**, 538–542.
9. Ayala, Y.M., Pantano, S., D'Ambrogio, A., Buratti, E., Brindisi, A., Marchetti, C., Romano, M. and Baralle, F.E. (2005) Human Drosophila, and *C. elegans* TDP43: nucleic acid binding properties and splicing regulatory function. *J. Mol. Biol.*, **348**, 575–588.
10. Gitler, A.D. and Shorter, J. (2011) RNA-binding proteins with prion-like domains in ALS and FTL-D. *Prion*, **5**, 179–187.
11. Da Cruz, S. and Cleveland, D.W. (2011) Understanding the role of TDP-43 and FUS/TLS in ALS and beyond. *Curr. Opin. Neurobiol.*, **21**, 904–919.

12. Lee, E.B., Lee, V.M.Y. and Trojanowski, J.Q. (2012) Gains and losses: molecular mechanisms of TDP43-mediated neurodegeneration. *Nat. Rev. Neurosci.*, **13**, 38–50.
13. Buratti, E. and Baralle, F.E. (2010) The multiple roles of TDP-43 in pre-mRNA processing and gene expression regulation. *RNA Biol.*, **7**, 420–429.
14. Węgorzewska, I. and Baloh, R.H. (2011) TDP-43 based animal models of neurodegeneration: new insights into ALS pathology and pathophysiology. *Neurodegenerat. Dis.*, **8**, 262–274.
15. Sephton, C.F., Cenik, C., Kucukural, A., Dammer, E.B., Cenik, B., Han, Y., Dewey, C.M., Roth, F.P., Herz, J., Peng, J. *et al.* (2011) Identification of neuronal RNA targets of TDP-43-containing ribonucleoprotein complexes. *J. Biol. Chem.*, **286**, 1204–1215.
16. Tollervey, J.R., Curk, T., Rogelj, B., Briese, M., Cereda, M., Kayikci, M., König, J., Hortobágyi, T., Nishimura, A.L., Zupunski, V. *et al.* (2011) Characterizing the RNA targets and position-dependent splicing regulation by TDP-43. *Nat. Neurosci.*, **14**, 452–458.
17. Polymenidou, M., Lagier-Tourenne, C., Hutt, K.R., Huelga, S.C., Moran, J., Liang, T.Y., Ling, S.C., Sun, E., Wanczewicz, E., Mazur, C. *et al.* (2011) Long pre-mRNA depletion and RNA missplicing contribute to neuronal vulnerability from loss of TDP-43. *Nat. Neurosci.*, **14**, 459–468.
18. Lagier-Tourenne, C., Polymenidou, M., Hutt, K.R., Vu, A.Q., Baughn, M., Huelga, S.C., Clutario, K.M., Ling, S.C., Liang, T.Y., Mazur, C. *et al.* (2012) Divergent roles of ALS-linked proteins FUS/TLS and TDP-43 intersect in processing long pre-mRNAs. *Nat. Neurosci.*, **15**, 1488–1497.
19. Lukacsovich, T., Asztalos, Z., Juni, N., Awano, W. and Yamamoto, D. (1999) The *Drosophila melanogaster* 60A chromosomal division is extremely dense with functional genes: their sequences, genomic organization, and expression. *Genomics*, **57**, 43–56.
20. Zhou, Q., Zhang, G., Zhang, Y., Xu, S., Zhao, R., Zhan, Z., Li, X., Ding, Y., Yang, S. and Wang, W. (2008) On the origin and evolution of new genes in *Drosophila*. *Genome Res.*, **18**, 1446–1455.
21. Strong, M.J., Volkening, K., Hammond, R., Yang, W., Strong, W., Leystra-Lantz, C. and Shoesmith, C. (2007) TDP43 is a human low molecular weight neurofilament (hNFL) mRNA-binding protein. *Mol. Cell Neurosci.*, **35**, 320–327.
22. Ayala, Y.M., Zago, P., D'Ambrogio, A., Xu, Y.F., Petrucelli, L., Buratti, E. and Baralle, F.E. (2008) Structural determinants of the cellular localization and shuttling of TDP-43. *J. Cell Sci.*, **121**, 3778–3785.
23. White, K.E., Humphrey, D.M. and Hirth, F. (2010) The dopaminergic system in the aging brain of *Drosophila*. *Front. Neurosci.*, **4**, 205–333.
24. Humphrey, D.M., Parsons, R.B., Ludlow, Z.N., Riemensperger, T., Esposito, G., Verstreken, P., Jacobs, H.T., Birman, S. and Hirth, F. (2012) Alternative oxidase rescues mitochondria-mediated dopaminergic cell loss in *Drosophila*. *Hum. Mol. Genet.*, **21**, 2698–2712.
25. Strauss, R. (2002) The central complex and the genetic dissection of locomotor behaviour. *Curr. Opin. Neurobiol.*, **12**, 633–638.
26. Fiesel, F.C., Voigt, A., Weber, S.S., Van den Haute, C., Waldenmaier, A., Görner, K., Walter, M., Anderson, M.L., Kern, J.V., Rasse, T.M. *et al.* (2010) Knockdown of transactive response DNA-binding protein (TDP-43) downregulates histone deacetylase 6. *EMBO J.*, **29**, 209–221.
27. Feiguin, F., Godena, V.K., Romano, G., D'Ambrogio, A., Klima, R. and Baralle, F.E. (2009) Depletion of TDP-43 affects *Drosophila* motoneurons terminal synapses and locomotive behavior. *FEBS Lett.*, **583**, 1586–1592.
28. Lin, M.J., Cheng, C.W. and Shen, C.K. (2011) Neuronal function and dysfunction of *Drosophila* dTDP. *PLoS One*, **6**, e20371.
29. Godena, V.K., Romano, G., Romano, M., Appocher, C., Klima, R., Buratti, E., Baralle, F.E. and Feiguin, F. (2011) TDP-43 regulates *Drosophila* neuromuscular junctions growth by modulating Futsch/ MAP1B levels and synaptic microtubule organization. *PLoS One*, **6**, e17808.
30. Wang, J.W., Brent, J.R., Tomlinson, A., Shneider, N.A. and McCabe, B.D. (2011) The ALS-associated proteins FUS and TDP-43 function together to affect *Drosophila* locomotion and life span. *J. Clin. Invest.*, **121**, 4118–4126.
31. Collins, C.A. and DiAntonio, A. (2007) Synaptic development: insights from *Drosophila*. *Curr. Opin. Neurobiol.*, **17**, 35–42.
32. Kitamoto, T. (2001) Conditional modification of behaviour in *Drosophila* by targeted expression of a temperature-sensitive *shibire* allele in defined neurons. *J. Neurobiol.*, **47**, 81–92.
33. Dietzl, G., Chen, D., Schnorrer, F., Su, K.C., Barinova, Y., Fellner, M., Gasser, B., Kinsey, K., Oettel, S., Scheiblauer, S. *et al.* (2007) A genome-wide transgenic RNAi library for conditional gene inactivation in *Drosophila*. *Nature*, **448**, 151–156.
34. Budnik, V., Koh, Y.H., Guan, B., Hartmann, B., Hough, C., Woods, D. and Gorczyca, M. (1996) Regulation of synapse structure and function by the *Drosophila* tumor suppressor gene *dlg*. *Neuron*, **17**, 627–640.
35. Hirth, F. (2010) *Drosophila melanogaster* in the study of human neurodegeneration. *CNS Neurol. Disord. Drug Targets*, **9**, 504–523.
36. Nicolai, L.J., Ramaekers, A., Ramaekers, T., Drozdzecki, A., Mauss, A.S., Yan, J., Landgraf, M., Annaert, W. and Hassan, B.A. (2010) Genetically encoded dendritic marker sheds light on neuronal connectivity in *Drosophila*. *Proc. Natl Acad. Sci. USA*, **107**, 20553–20558.
37. Raff, M.C., Whitmore, A.V. and Finn, J.T. (2002) Axonal self-destruction and neurodegeneration. *Science*, **296**, 868–871.
38. Fischer, L.R., Culver, D.G., Tennant, P., Davis, A.A., Wang, M., Castellano-Sanchez, A., Khan, J., Polak, M.A. and Glass, J.D. (2004) Amyotrophic lateral sclerosis is a distal axonopathy: evidence in mice and man. *Exp. Neurol.*, **185**, 232–240.
39. Boll, W. and Noll, M. (2002) The *Drosophila Pox neuro* gene: control of male courtship behaviour and fertility by a complete dissection of all enhancers. *Development*, **129**, 5667–5681.
40. Ayala, Y.M., De Conti, L., Avendaño-Vázquez, S.E., Dhir, A., Romano, M., D'Ambrogio, A., Tollervey, J., Ule, J., Baralle, M., Buratti, E. *et al.* (2011) TDP-43 regulates its mRNA levels through a negative feedback loop. *EMBO J.*, **30**, 277–288.
41. Igaz, L.M., Kwong, L.K., Lee, E.B., Chen-Plotkin, A., Swanson, E., Unger, T., Malunda, J., Xu, Y., Winton, M.J., Trojanowski, J.Q. *et al.* (2011) Dysregulation of the ALS-associated gene TDP-43 leads to neuronal death and degeneration in mice. *J. Clin. Invest.*, **121**, 726–738.
42. Ritson, G.P., Custer, S.K., Freibaum, B.D., Guinto, J.B., Geffel, D., Moore, J., Tang, W., Winton, M.J., Neumann, M., Trojanowski, J.Q. *et al.* (2010) TDP-43 mediates degeneration in a novel *Drosophila* model of disease caused by mutations in VCP/p97. *J. Neurosci.*, **30**, 7729–7739.
43. Miguel, L., Frébourg, T., Campion, D. and Lecourtis, M. (2010) Both cytoplasmic and nuclear accumulations of the protein are neurotoxic in *Drosophila* models of TDP-43 proteinopathies. *Neurobiol. Dis.*, **41**, 398–406.
44. Guo, W., Chen, Y., Zhou, X., Kar, A., Ray, P., Chen, X., Rao, E.J., Yang, M., Ye, H., Zhu, L. *et al.* (2011) An ALS-associated mutation affecting TDP-43 enhances protein aggregation, fibril formation and neurotoxicity. *Nat. Struct. Mol. Biol.*, **18**, 822–830.
45. Xu, Y.F., Gendron, T.F., Zhang, Y.J., Lin, W.L., D'Alton, S., Sheng, H., Casey, M.C., Tong, J., Knight, J., Yu, X. *et al.* (2010) Wild-type human TDP-43 expression causes TDP-43 phosphorylation, mitochondrial aggregation, motor deficits, and early mortality in transgenic mice. *J. Neurosci.*, **30**, 10851–10859.
46. Shan, X., Chiang, P.M., Price, D.L. and Wong, P.C. (2010) Altered distributions of Gemini of coiled bodies and mitochondria in motor neurons of TDP-43 transgenic mice. *Proc. Natl Acad. Sci. USA*, **107**, 16325–16330.
47. Kuo, P.H., Doudeva, L.G., Wang, Y.T., Shen, C.K. and Yuan, H.S. (2009) Structural insights into TDP-43 in nucleic-acid binding and domain interactions. *Nucleic Acids Res.*, **37**, 1799–1808.
48. Freibaum, B.D., Chitta, R.K., High, A.A. and Taylor, J.P. (2010) Global analysis of TDP-43 interacting proteins reveals strong association with RNA splicing and translation machinery. *J. Proteome Res.*, **9**, 1104–1120.
49. Kim, S.H., Shanware, N.P., Bowler, M.J. and Tibbetts, R.S. (2010) Amyotrophic lateral sclerosis-associated proteins TDP-43 and FUS/TLS function in a common biochemical complex to co-regulate HDAC6 mRNA. *J. Biol. Chem.*, **285**, 34097–34105.
50. Ling, S.C., Albuquerque, C.P., Han, J.S., Lagier-Tourenne, C., Tokunaga, S., Zhou, H. and Cleveland, D.W. (2010) ALS-associated mutations in TDP-43 increase its stability and promote TDP-43 complexes with FUS/TLS. *Proc. Natl Acad. Sci. USA*, **107**, 13318–13323.
51. Mehnert, K.I., Beramendi, A., Elghazali, F., Negro, P., Kyriacou, C.P. and Cantera, R. (2007) Circadian changes in *Drosophila* motor terminals. *Dev. Neurobiol.*, **67**, 415–421.
52. Conforti, L., Adalbert, R. and Coleman, M.P. (2007) Neuronal death: where does the end begin? *Trends Neurosci.*, **30**, 159–166.
53. Osterloh, J.M., Yang, J., Rooney, T.M., Fox, A.N., Adalbert, R., Powell, E.H., Sheehan, A.E., Avery, M.A., Hackett, R., Logan, M.A. *et al.* (2012) dSarm/Sarm1 is required for activation of an injury-induced axon death pathway. *Science*, **337**, 481–484.

54. Azzouz, M., Leclerc, N., Gurney, M., Warter, J.M., Poindron, P. and Borg, J. (1997) Progressive motor neuron impairment in an animal model of familial amyotrophic lateral sclerosis. *Muscle Nerve*, **20**, 45–51.
55. Pasinelli, P. and Brown, R.H. (2006) Molecular biology of amyotrophic lateral sclerosis: insights from genetics. *Nat. Rev. Neurosci.*, **7**, 710–723.
56. Zhang, Y.Q., Rodesch, C.K. and Broadie, K. (2002) Living synaptic vesicle marker: synaptotagmin-GFP. *Genesis*, **34**, 142–145.
57. Wang, J., Zugates, C.T., Liang, I.H., Lee, C.H. and Lee, T. (2002) Drosophila Dscam is required for divergent segregation of sister branches and suppresses ectopic bifurcation of axons. *Neuron*, **33**, 559–571.
58. Estes, P.S., Boehringer, A., Zwick, R., Tang, J.E., Grigsby, B. and Zarnescu, D.C. (2011) Wild-type and A315T mutant TDP-43 exert differential neurotoxicity in a Drosophila model of ALS. *Hum. Mol. Genet.*, **20**, 2308–2321.
59. Horn, T. and Boutros, M. (2010) E-RNAi: a web application for the multi-species design of RNAi reagents—2010 update. *Nucl. Acids Res.*, **38**, W332–W339.
60. Bischof, J., Maeda, R.K., Hediger, M., Karch, F. and Basler, K. (2007) An optimized transgenesis system for Drosophila using germ-line-specific phiC31 integrases. *Proc. Natl. Acad. Sci. USA*, **104**, 3312–3317.
61. Brent, J.R., Werner, K.M. and McCabe, B.D. (2009) Drosophila Larval NMJ Dissection. *J. Vis. Exp.*, **24**, e1107.
62. Straw, A.D. and Dickinson, M.H. (2009) Motmot, an open-source toolkit for realtime video acquisition and analysis. *Source Code Biol. Med.*, **4**, 5.
63. Branson, K., Robie, A.A., Bender, J.A., Perona, P. and Dickinson, M.H. (2009) High-throughput ethomics in large groups of Drosophila. *Nat. Methods*, **6**, 451–457.
64. Elliott, C.J.H. and Sparrow, J.C. (2012) In vivo measurement of muscle output in intact Drosophila. *Methods*, **56**, 78–86.
65. Stewart, B.A., Atwood, H.L., Renger, J.J., Wang, J. and Wu, C.F. (1994) Improved stability of Drosophila larval neuromuscular preparations in haemolymph-like physiological solutions. *J. Comp. Physiol. A*, **175**, 179–191.
66. Heisenberg, M. (1971) Separation of receptor and lamina potentials in the electroretinogram of normal and mutant Drosophila. *J. Exp. Biol.*, **55**, 85–100.